Fates of satellite ejecta in the Saturn system, II

José Luis Alvarellos[a,*], Anthony R. Dobrovolskis[b], Kevin J. Zahnle[c], Patrick Hamill[d], Luke Dones[e], Stuart Robbins[e]

[a] SSL, 3825 Fabian Way, MS G-76, Palo Alto, California 94303, United States
[b] SETI Institute, MS 245-3, Moffett Field, California 94035, United States
[c] NASA Ames Research Center, MS 245-3, Moffett Field, California 94035, United States
[d] Department of Physics, San José State University, San José, California 95192, United States
[e] Southwest Research Institute, 1050 Walnut Street, Suite 300, Boulder, CO 80302, United States

A B S T R A C T

We assess the fates of ejecta from the large craters Aeneas on Dione and Ali Baba on Enceladus (161 and 39 km in diameter, respectively), as well as that from Herschel (130 km in diameter) on Mimas. The ejecta are treated either as 'spalls' launched from hard surfaces, or as 'rubble' launched from a weak rubble pile regolith. Once in orbit we consider the ejecta as massless test particles subject to the gravity of Saturn and its classical satellites. The great majority of escaped ejecta get swept up by the source moons. The best fit to the ejecta population decay is a stretched exponential with exponent near 1/2 (Dobrovolskis et al., Icarus 188, 481–505, 2007). We bracket the characteristic ejecta sizes corresponding to Grady–Kipp fragments and spalls. Based on this and computed impact velocities and incidence angles, the resulting sesquinary craters, if they exist, should have diameters on the order of a few meters to a few km. The observed longitude distribution of small craters on Mimas along with the findings of Bierhaus et al. that small moons should not have a secondary crater population (Icarus 218, 602–621, 2012) suggest that the most likely place to find sesquinary craters in the Saturn system is the antapex of Mimas.

© 2016 Elsevier Inc. All rights reserved.

1. Introduction and previous work

Mimas, Enceladus and Dione are three of the classical icy satellites of Saturn. The orbits of the latter two moons are dynamically linked in a 2:1 mean motion resonance (Harper and Taylor, 1993; Sinclair, 1972). Intrinsically, these small worlds are very interesting in their own right (Buratti, 1999; Moore and Hunt, 1983; Morrison et al., 1986). Even though Enceladus is among the smallest of Saturn's classical satellites, it is geologically active: it has geysers on its south pole continually spewing particles that feed Saturn's E-ring (Spencer, 2011). For the most part these particles are water ice, but there are other simple dissolved compounds (Waite et al., 2009), as well as nm-sized, silicon-rich grains (Hsu et al., 2015). For its part, Mimas is the smallest and innermost of the classical icy satellites, and in Herschel it has such a large impact crater that the comet which produced it probably came close to shattering this moon (Moore and Hunt, 1983; Smith, 1981). Dione is outwardly similar to Tethys, albeit with a diameter about 6% larger and a higher density. Some of its most distinctive features are the

ice cliffs on its trailing hemisphere, created by fractures on the surface that were first seen as bright, linear features on Voyager images (the so-called 'wispy terrain'). A feature of Dione is that its trailing hemisphere is its most heavily cratered, contrary to expectations that the leading hemisphere would be most cratered if the impactors were solely heliocentric comets (Horedt and Neukum, 1984; Shoemaker and Wolfe, 1982; Zahnle et al., 1998). With the exceptions of Hyperion and Phoebe, all of the classical satellites of Saturn are tidally locked.

1.1. Previous work

We previously investigated the fate of ejecta resulting from some of the largest craters on icy satellites of Saturn (Alvarellos et al., 2005, AZDH henceforth). The motivating factor was to test the hypothesis of Smith (1981, 1982) that the small craters on the icy saturnian moons, the so-called Population II craters, were formed by escaped impact ejecta that had come back after spending some time in planetocentric orbit (i.e., *sesquinary* craters; Dobrovolskis and Burns, 1980; Dobrovolskis and Lissauer, 2004). Specific initial conditions were produced for ejecta from crater Herschel on Mimas; craters Odysseus and Penelope on Tethys; and crater Tirawa on Rhea (AZDH). These craters are very large and,

since these lie on relatively small moons, the impacts that made them are expected to throw out large amounts of mass into orbit about Saturn.

The escaping ejecta were treated as massless test particles subject to the gravitational perturbations of Saturn and its oblateness terms, the gravitational perturbations of the classical satellites (Mimas-Phoebe) and the Sun. Trajectories were integrated forward in time using the Swift RMVS3 algorithm of Levison and Duncan (1994). The launch parameters followed two slightly different ejection models: the spallation model of Melosh (1984) and a rubble model based on the work of Housen et al. (1983). These models are described in detail in the original sources and in our implementation of them (AZDH). Since the ejecta start on orbits that intersect the path of the source moon, the majority of them return to the source moon after some time (years to hundreds or thousands of years). Indeed, AZDH found that the fraction of escaped ejecta that returns ranges between 81.5% and 99.6%, depending on the ejection model and source moon. The rest either survive the integrations, or more likely, reach other moons, with those moons on adjacent orbits to the source satellite more likely to get hit than the more distant ones. Escaping ejecta thrown out from craters near the apex of the satellite's motion and which do not come back to the source moon are more likely to reach moons in outer orbits, whilst ejecta launched from near the antapex are more likely to hit inner moons.

When an ejectum struck the source moon, we recorded its impact speed and angle, as well as the latitude and longitude of its point of impact. Besides the initial conditions for the ejecta particles, we also assigned them sizes according to Melosh (1984). With this information we estimated the crater sizes these ejecta made when they hit various targets. Our conclusion was that planetocentric debris could create craters a few km in diameter in most cases, with the largest crater in our simulations being 19 km across.

Since then a number of studies relevant to this subject have been published. Dobrovolskis et al. (2007) determined that the original population of escaped ejecta, which forms a 'swarm' of debris orbiting the central planet, decays as a 'stretched exponential' function, with a growing half-life. In a pair of related papers, Alvarellos et al. (2008) and Zahnle et al. (2008) explored the possibility of ejecta due to impacts on Io reaching Europa. In AZDH we assumed the size of the ejecta to range between the spall-plate thickness and the average spall dimension. Zahnle et al. (2008) further constrained the size range of the ejecta to lie between the Grady–Kipp fragment size and the spall-plate thickness. In addition, Zahnle et al. (2008) clarified the correct expression to use for the particle velocity in the spall model, a correction we apply in this paper.

Kirchoff and Schenk (2010) studied crater distributions on Mimas, Tethys, Dione, Rhea and Iapetus from Cassini data. They found that the crater distributions on Mimas, Tethys and Dione are consistent with two impacting populations as originally described by Smith (1981). Leliwa-Kopystynski et al. (2011) studied the observed longitudinal distribution of craters on icy satellites of Jupiter (Ganymede and Callisto) and Saturn (Mimas, Tethys, Dione, Rhea and Iapetus). Most of the satellites studied show longitudinal asymmetries; interestingly, the distribution of small craters on Mimas measured by Leliwa-Kopystynski et al. (2011, Fig. 2) is very similar to that predicted by AZDH (Fig. 12 therein) for debris originating from the giant crater Herschel.

Finally, Bierhaus et al. (2012, BDAZ henceforth) calculate the total amount of mass thrown out for a given impact and show that small moons such as Mimas are not expected to show evidence of secondary cratering because of their weak gravities. In general, the

Table 1

Properties of Mimas, Enceladus and Dione. Here we tabulate the satellite's semi-major axes, orbital speed and period; its bulk density; its physical and Hill radii R_m and R_H, as well as their ratio χ; the classical and effective escape velocities v_{esc} and v_{esc}^* (assuming $\alpha = 45°$); the acceleration of gravity at the satellite's surface; the transition diameter from simple to complex crater (Zahnle et al., 2003); and the strength to gravity transition diameter D_{sg}. Note that since D_{sg} is a function of impact speed, the values are given in terms of range appropriate for infalling ejecta impact speeds; see text for details.

Satellite	Mimas	Enceladus	Dione
Semi-major axis (km)	185,520	238,020	377,400
Orbital speed, v_{orb} (km/s)	14.3	12.6	10.0
Orbital period, T (days)	0.94	1.37	2.74
Bulk density, ρ_m (gm/cm^3)	1.15	1.61	1.46
Physical radius, R_m (km)	198	252	562
Hill radius, R_H (km)	521	950	3259
$\chi \equiv R_m/R_H$	0.380	0.265	0.172
Classical escape speed, v_{esc} (m/s)	159	239	510
Effective escape speed, v_{esc}^* (m/s)	130	209	467
Acceleration at the surface, g (cm/s^2)	6.4	11.3	23.2
Simple to complex transition crater diameter, D_c (km)	15.0	15.0	15.0
Strength to gravity transition crater diameter, D_{sg} (km)	17.2–47.1	10.4–22.7	3.5–7.2

of Saturn are expected to have both secondaries and sesquinary craters, while larger worlds such as the Galilean moons, as well as the Moon, Mercury and Mars, are expected to have vast numbers of secondary craters (Bierhaus and Dones, 2012).

In this paper we extend the work of AZDH to Enceladus and Dione and present new insights based on other work. The objective of this investigation is to determine whether the shape of the distributions of small craters on icy satellites, as seen in R-plots, can be explained by satellite fragments generated by ecliptic comets as they collide with a moon. In Table 1 we present basic properties for the three satellites of Saturn we consider in this paper: Mimas, Enceladus and Dione. In Section 2 we present the results of simulations of ejecta from Enceladus, while in Section 3 we do the same for ejecta from Dione. In Section 4 we revisit the case of Mimas ejecta. Finally in Section 5 we provide a discussion and state our conclusions.

2. Ejecta from Enceladus

The most common impactors on regular satellites in the outer Solar System are ecliptic comets (see Dones et al., 2009; Zahnle et al., 2003; 2001) which are responsible for most primary craters in the outer Solar System. Generally speaking, the formation of relatively large craters is dominated by gravity; in contrast, the formation of small craters is driven by the strength of the target material (gravity and strength regimes, respectively; Chapman and McKinnon, 1986). At 39.2 km in diameter Ali Baba is one of the largest craters on Enceladus (see Table 2). It is located on the northern hemisphere of the Saturn-facing side and has been known since the Voyager flybys (Moore and Hunt, 1983). We will investigate the fate of ejecta from this crater.

2.1. Cratering in the gravity regime

Following the work of Zahnle et al. (2003, 2008), and Alvarellos et al. (2008), we adopt the following expression for the diameter of a transient/apparent crater (the temporary crater created at the end of the excavation stage in the cratering process; see Chapman and McKinnon, 1986) in the gravity regime:

mass available to make secondary craters depends on the relative values of the escape speed and $v_{\min}$, the minimum speed needed to make secondaries (BDAZ). The other larger classical icy moons

$$D_a = 1.1 \left(\frac{U^2}{gd} \right)^{0.217} \left(\frac{\rho_i \sin \alpha}{\rho_t} \right)^{0.333} d, \tag{1}$$

Table 2
Crater data and impact speeds for ecliptic comets presumed to have produced craters Herschel, Ali Baba and Aeneas. Latitude and longitude are from Batson (1984). The transient crater diameter D_a is obtained from Eq. (2); Δ is the angular distance of the crater from the apex of motion in degrees, while U is the expected impact speed of the ecliptic comet that made the given crater. Estimated radii of the impactors are listed in the row labeled $d/2$.

Crater satellite	Herschel Mimas	Ali Baba Enceladus	Aeneas Dione
Observed diameter, D (km)	130.0	39.2	161.0
Transient diameter, D_a (km)	101.4	35.1	122.6
Latitude (degrees)	0.0	55.1	25.9
Longitude (degrees)	−104.0	−22.3	−46.3
Δ (degrees)	14.0	77.4	48.4
Impactor speed U (km/s)	30.0	23.2	20.4
Impactor radius $d/2$ (km)	2.3	0.8	5.3

Table 3
More parameters used in this paper. The value of σ_t is from Zahnle et al. (2008).

Quantity	Symbol	Value
Impactor density (g/cm^3)	ρ_i	0.6
Target density (g/cm^3)	ρ_t	0.9
Seismic speed (km/s)	C_L	2.0
Tensile strength (Pascals)	σ_t	1.0×10^7

where g is the local acceleration of gravity at the target surface; U is the relative velocity of impact; ρ_i and ρ_t are the impactor density and target crustal density, respectively; α is the incidence angle measured from the horizontal; and d is the impactor diameter. U depends on the angular distance of the impact site from the target moon's apex of motion, and on that moon's orbital distance and speed, as well as on the impactor's velocity 'at infinity' (that is, its heliocentric orbital velocity with respect to Saturn's); see Zahnle et al. (2001) and AZDH. The expression above for crater size is consistent with rock, wet sand, and water (Housen and Holsapple, 2011; Schmidt and Housen, 1987). Craters smaller than a critical diameter D_c retain a simple bowl shape, but larger craters turn into complex craters (Chapman and McKinnon, 1986). For Enceladus we assume $D_c = 15$ km (Zahnle et al., 2003, see Table 2). For $D_a > 15$ km the final, observed crater diameter D is given by

$$D = D_a (D_a/D_c)^{0.13} \tag{2}$$

(Zahnle et al., 2003), while for $D_a \leq 15$ km, $D = D_a$. Note that for Ali Baba, $D > D_c$. Based on the work of Zahnle et al. (2003, 2001), assuming an incidence angle of 45° (the most probable incidence angle; Gilbert, 1893; Shoemaker and Wolfe, 1982), and assuming cometary and target densities of 0.6 and 0.9 g/cm^3, respectively (see Table 3 for a listing of further parameters), we estimate that the comet that generated this crater was traveling at 23.2 km/s (AZDH, Eq. (4)) and its diameter $d = 1.6$ km (i.e., $m_i \approx 10^{12}$ kg).

2.2. Ejected mass

Following BDAZ, the total ejected mass is given by

$$M_{tot} = 3.75 \times 10^{-2} \rho_t D_a^3 \tag{3}$$

A total of 1.5×10^{15} kg of mass was ejected when this crater was made, or three orders of magnitude more than the impactor mass. Based on the work of Housen and Holsapple (2011), BDAZ calculated that the amount of ejecta mass that escapes an icy satellite

speed) is

$$v_{esc}^* = v_{esc} \sqrt{\frac{1 - \chi}{1 - \chi^2 \cos^2 \alpha}} \tag{5}$$

(Alvarellos et al., 2002, AZDH; Dobrovolskis et al., 2010), where $\chi = R_m/R_H$ is the ratio of the moon's radius to its Hill radius; for Enceladus, $v_{esc}^* = 209$ m/s or about 87% of v_{esc}; see Table 1. For Ali Baba, the amount of escaping mass is approximately $M_{esc} = 3.5 \times 10^{12}$ kg, or about two and a half times the impactor mass. Zahnle et al. (2008) estimated that $M_{esc} = 3m_i$, so these results are consistent.

This then represents the basic setting for our integrations: a comet strikes Enceladus and creates a crater (Ali Baba), of which only about 0.2% of the ejecta have enough energy to escape into orbit about Saturn. What happens to the other 99.8% of the ejected mass? BDAZ studied the secondary crater fields surrounding the Europan craters Rhiannon and Tyre; more specifically, they recorded distances of the proximal secondaries. Applying appropriate ballistic equations to solve for the speeds needed to reach those minimum distances, BDAZ suggested the empirical result that the minimum speed needed to create secondary craters on icy satellites lies in the range 150 m/s $< v_{\min} < 250$ m/s (with a caveat that the uncertainty in the lower end is higher than in the upper end). The mass available to make secondary craters is then given by (BDAZ)

$$M_{sec} = M(v_{\min}) - M_{esc} \tag{6}$$

where $M(v_{\min})$ is the amount of mass ejected faster than $v_{\min}$, given by Eq. (4), but substituting $v_{\min}$ for v_{esc}^*. Mass ejected faster than $v_{\min}$ but slower than v_{esc}^* is available to make secondary craters. If $v_{\min} > v_{esc}^*$ no mass is available to make secondary craters and the total ejected mass is partitioned between the ejecta blanket (the vast majority) and mass available to make sesquinary craters (BDAZ). For ejecta from Ali Baba, if $v_{\min} = 150$ m/s, then approximately 2.0×10^{12} kg of mass is available to produce secondary craters; however, if $v_{\min} = 250$ m/s then **no** mass is available for secondary craters. BDAZ clarified that the amount of mass available to make secondary craters is related to the difference between v_{esc}^* and $v_{\min}$; an important finding is that for the smaller, icy moons Enceladus and Mimas, very little, if any, mass is available to make secondary craters.

Most of the ejected mass ends up in the crater ejecta blanket (BDAZ):

$$M_{eb} = M_{tot} - M(v_{\min}) \tag{7}$$

where M_{eb} is the mass of the ejecta blanket. In Table 4 we summarize these findings for Enceladus; compare with Table 2 from BDAZ.

2.3. Ejecta size

Following concepts and nomenclature introduced by Melosh (1984), Zahnle et al. (2008) argued that the natural size scales to use to compute ejecta size are the spall-plate thickness Z_s and the Grady–Kipp fragment size L_{GK}. The former is approximately given by (Melosh, 1985)

$$Z_s = \frac{\sigma_t d}{\rho_t C_L v_{ej}}, \tag{8}$$

without an atmosphere is given by

$$M_{esc} = 6.7 \times 10^{-3} m_i \left(\frac{U \sin \alpha}{v_{esc}^*} \right)^{1.38} \left(\frac{\rho_i}{\rho_t} \right)^{0.2} \qquad (4)$$

where v_{esc}^* is the effective escape speed needed to reach Enceladus' Hill sphere. The relationship between v_{esc}^* and v_{esc} (classical escape

where d is the impactor diameter, σ_t represents the tensile strength and C_L represents the longitudinal speed of sound of the target material, while v_{ej} is the ejection velocity; see Table 3 for the numerical values. Spallation is a process whereby competent (i.e., hard rock or cold ice), relatively lightly shocked target material can be ejected at high speeds. The morphology of such ejecta

Table 4
The total and fractional masses for crater Ali Baba (on Enceladus) and resulting ejecta for two possible values of v_{min} (minimum speed needed to make secondary craters). The total mass ejected is $M_{tot} = 1.461 \times 10^{15}$ kg. The quantity v_{min} was defined in Section 2.2. Subscripts 'eb' and 'sec' refer to ejecta blanket and secondaries respectively. Subscript 'esc' refers to the amount of mass that escapes Enceladus to go into orbit about Saturn, and is therefore potentially available to make sesquinary craters. Note that (a) for the case $v_{min} = 150$ m/s the fractions do not add exactly to 1.0 due to rounding, and (b) for the case $v_{min} = 250$ m/s no mass is available to make secondary craters.

v_{min} (m/s)	M_{eb} (kg)	f_{eb}	M_{sec} (kg)	f_{sec}	M_{esc} (kg)	f_{esc}
150	1.455×10^{15}	0.996	2.012×10^{12}	0.001	3.488×10^{12}	0.002
250	1.458×10^{15}	0.998	0.0	0.000	3.488×10^{12}	0.002

blocks is peculiar: spall-plates roughly resemble slabs where the width and height can be several to tens of times their thickness.

The Grady–Kipp fragments represent highly shocked material lying deeper in the target, under the spall plates. Their size is smaller, and is given by

$$L_{GK} = \frac{\sigma_t d}{\rho_t v_{ej}^{2/3} U^{4/3}}, \qquad (9)$$

A third scale is that intrinsic to the target material – e.g., for Io, a third scale might be the thickness of the individual lava flows. We know of no comparable scales intrinsic to icy satellites, but we would not rule out the possibility that there may be such scales.

2.4. Initial conditions

In this paper we are mostly concerned with the small fraction of ejected mass that escapes a moon, in this case Enceladus (i.e., particles with ejection speed $v_{ej} > v_{esc}^*$). We use the given impact event characteristics to create initial conditions for massless test particles representing the escaping ejecta, as was done by AZDH. We adopt two models for the ejecta initial conditions: (a) the spallation (stress-wave) model of Melosh (1984) and (b) the 'rubble' model (Housen et al., 1983); both models are discussed in AZDH and references therein. In brief, the spallation model produces slightly higher ejection speeds and a variety of ejection angles (the closer to the center of the impact, the more nearly vertical is the ejection). We assigned fixed 45° ejection angles to the model of Housen et al. (1983) and called it the 'rubble' model. Hence, dependency on launch angles is tested between spalls and rubble ejecta; however, elsewhere we showed that the fate of the ejected particles is not a strong function of the ejection angle (see Alvarellos et al., 2002, Fig. 13). For the spall model, however, we use the expression for the particle velocity from Zahnle et al. (2008, Eq. (14)). The test particle initial conditions are computed in a topocentric coordinate system, which is then mapped to a planetocentric coordinate system. Note that for a given impact all parameters in Eqs. (8) and (9) are single-valued, except for v_{ej}. Our algorithms provide a set of ejection speeds that range from the slowest ejecta barely able to escape the satellite's gravity to the fastest ejecta (ejected near the edge of the impactor; see AZDH Figs. 2 and 3). For Enceladus spall ejecta we obtain $v_{esc}^* < v_{ej} < 1.46$ km/s while for rubble ejecta we obtain $v_{esc}^* < v_{ej} < 0.96$ km/s.

These initial conditions, along with initial conditions for the Saturn system and its airless, icy moons are then fed to the Swift/RMVS3 (Regularized, Mixed-Variable Symplectic) numerical

perturber (satellite initial conditions were provided by R. Jacobson -personal communication). Other perturbations taken into account are the gravity of Saturn and its oblateness terms (the time-step for these integrations is 19.7 minutes). Given that gravitational perturbations from an external object 'A' of mass m_A on an interior object 'B' are proportional to m_A and inversely proportional to the **cube** of the ratio in semi-major axes of body 'A' and 'B', we expect that results of the two runs (simplified and full systems) to be qualitatively the same, while quantitatively different; for instance, using values from Table 1 we see that the perturbation strength at Enceladus due to Dione is approximately 1.5× that due to Mimas. There are 2400 test particles ejected per crater (600 assuming spalls, 600 assuming the rubble model each for the simplified and full systems). These test particles are a representative subset of the actual number of particles N ejected during an actual impact, where N is on the order of perhaps 10^6 to 10^8 (Zahnle et al., 2008).

The code has also been modified to detect collisions with the rings (as was done by Dobrovolskis and Lissauer, 2004). Swift will remove a particle if any of the following conditions are met: (a) if at a given time-step the particle is found to be located 'inside' a massive body; (b) if the particle will hit a massive body in the next time step; (c) if the particle's periapse distance from a moon is less than one satellite radius; and (d) if a particle encounters the rings. The few particles from the simulation which come back to Enceladus in less than twice its orbital period of 1.37 days are ignored for our purposes, because these represent particles on ballistic trajectories and/or temporary chaotic satellites which go almost all the way to the inner edge of Enceladus' Hill sphere but do not escape, see Alvarellos et al. 2002, AZDH.

2.5. Enceladus ejecta: results

Qualitatively, the results for all runs are very similar. The vast majority of escaping ejecta came back to Enceladus itself (> 98%); this is expected because these particles start on Enceladus-crossing orbits, which have a high probability of impacting their source moon (Burns and Gladman, 1998; Hamilton and Burns, 1994). In neither case were impacts on Saturn or its rings detected. Between 1.0 and 1.8% of the ejecta hit Tethys; note that this implies that between 3.5 and 6.3×10^{10} kg of Enceladus material reach Tethys. In the simplified 'rubble' run, the last particle was removed at 12,478 years. The simplified 'spalls' run had one surviving particle which lasted until at least 19,000 years. Results for all cases are summarized in Table 5; as can be seen, the 'simplified' and 'full system' run results are qualitatively very similar.

integrator ([Levison and Duncan, 1994](#)). The whole system is then integrated forward in time for 19,000 years in order to investigate the long-term fate of these ejecta from crater Ali Baba.

For both spalls and rubble we carried out two sets of simulations. The first is a simplified set (i.e., faster runtimes) consisting of the ejecta test particles plus the massive moons Mimas, Methone, Enceladus, Tethys, and its coorbitals Calypso and Telesto, and Dione. The second set consists of the aforementioned test particles and moons, plus Dione's coorbitals, as well as the rest of Saturn's classical satellites, and the Sun as the last, most distant

The decay of the orbiting ejecta population $P(t)$ is best described as a stretched-exponential law, also known as the Kohlrausch formula ([Dobrovolskis et al., 2007](#)):

$$P(t) = P_0 \exp\left(-[t/\tau]^\beta\right) \tag{10}$$

where P_0 is the initial population, τ is a time constant, and β is a dimensionless parameter; for $\beta = 1$ Eq. (10) reverts to a simple exponential decay. As was done in [Dobrovolskis et al. (2007)](#), several curve fits were tried and indeed the stretched-exponential decay provides the best fit for the Enceladus ejecta. These values,

Table 5

Fate of ejecta from crater Ali Baba (simulation time=19,000 years). N is the number of particles, while 'Perc.' means percentages, which have been normalized to the value labeled 'Escape' = 600 minus the number of suborbitals; 'Escape' represents the number of particles reaching saturnicentric orbit; see text for details. 'Active' means that the particles were still orbiting Saturn at the end of the integration. A dash ('-') in the columns for the simplified system means that the satellite in question was not included in the integration. Parameter fits to the stretched-exponential decay law (Eq. (10)) are listed at the bottom of the table.

	Simplified system				Full system			
	Rubble		Spalls		Rubble		Spalls	
Target	N	Perc.	N	Perc.	N	Perc.	N	Perc.
Saturn	0	0	0	0	0	0	0	0
Rings	0	0	0	0	0	0	0	0
Mimas	0	0	0	0	0	0	0	0
Methone	0	0	0	0	0	0	0	0
Enceladus	562	98.4%	563	98.6%	558	98.0%	564	98.8%
Tethys	9	1.6%	7	1.2%	10	1.8%	6	1.0%
Telesto	0	0	0	0	0	0	0	0
Calypso	0	0	0	0	0	0	0	0
Dione	0	0	0	0	0	0	0	0
Helene	–	–	–	–	0	0	0	0
Polydeuces	–	–	–	–	0	0	0	0
Rhea	–	–	–	–	0	0	0	0
Titan	–	–	–	–	0	0	0	0
Hyperion	–	–	–	–	0	0	0	0
Iapetus	–	–	–	–	0	0	0	0
Phoebe	–	–	–	–	0	0	0	0
Active	0	0	1	0.2%	1	0.2%	1	0.2%
Escape (P_0)	571	100%	571	100%	569	100%	571	100%
Parameter	τ (yrs)	β	τ (yrs)	β	τ (yrs)	β	τ (yrs)	β
Value	49.8	0.488	87.8	0.476	47.3	0.447	82.7	0.503
Uncertainty	± 11.8	± 0.018	± 21.2	± 0.015	± 13.0	± 0.187	± 25.2	± 0.208

as well as their estimated uncertainties, are shown at the bottom of Table 5. The values of β are quite similar, although the values for τ differ considerably. Note that for stretched exponential decay, the parameter τ represents the time at which the population has decayed to a value $1/e$ of the original population ([Dobrovolskis et al., 2007](#)). Unless otherwise stated, in the rest of what follows in Section 2 results are for the simplified system, given that it captures the essence of the behavior of the ejecta. In Fig. 1a we compare the actual decay of the initial population to the curve fits. Fig. 1b addresses the distribution of removal times from the simulation (rubble and spalls combined). Because the distribution of removal times is highly skewed to smaller removal times, we plot the logarithm of the removal time in order to see structure. The removals to the left of the black vertical line represent the suborbital ejecta, which are not taken into account in the analyses herein. The mean removal time for escaping Enceladus ejecta is 179 years, while the median removal time is 27 years. The mean time to get from Enceladus to Tethys was 267 years and the median time was 70 years, while the minimum time was 7 years.

At the time that a particle is removed from the integration, the state vectors of the massive system (that is, Saturn's moons) as well as the state vector of the removed particle are recorded and saved to a file by Swift. These planetocentric state vectors serve as initial conditions for a separate program which uses the Circular Restricted 3-Body Problem (CR3BP) as a model to determine

bution of impact latitudes is naturally concentrated near the equator, simply because latitude bands have less surface area as we get closer to the poles.

2.6. Crater size in the strength regime

For small craters, the critical parameter is the strength Y of the target material rather than local gravity. In this regime [Zahnle et al. (2008)](#) recommend the following expression for the transient/apparent crater size:

$$D_a = 1.9\left[\frac{mU^2 \sin\alpha}{Y}\right]^{1/3} \tag{11}$$

where m is the mass of the projectile/ejectum; as in [Zahnle et al. (2008)](#), we take $Y = \sigma_t$ (see Table 3).

To obtain the transition scale between strength and gravity regimes, we set Eqs. (1) and (11) equal and solve for the transition projectile diameter d_{sg}. To obtain the transition crater diameter D_{sg} we plug d_{sg} back into either Eqs. (1) or (11), then we find that $D_{sg} \propto g^{-1}U^{-0.36}$, that is, all other things being equal (same Y, ρ_t, α) D_{sg} is larger for smaller worlds and smaller impact velocities.

Using the aforementioned CR3BP code, we have computed estimates of the impact velocities and incidence angles for the returning ejecta. The impact velocities are approximately linearly corre-

where on the satellite the particle strikes, as well as its incidence angle and impact speed; details can be found in AZDH. In Fig. 2a we plot the impact sites (i.e., location of sesquinary craters) for particles which came back to Enceladus after orbiting Saturn. In AZDH we found that ejecta originating near the apex of motion of a synchronous satellite tend to come back near the antapex; conversely, ejecta originating near the antapex tend to come back near the apex. In this case, however, since Ali Baba is nowhere near these two points we expect the ejecta impact sites to be more or less randomly distributed in longitude; indeed, this is what is seen in Fig. 2b. The distribution of impact sites for ejecta from Ali Baba is akin to the distribution of impact sites we found for ejecta from crater Gilgamesh, on Ganymede (Alvarellos et al., 2002). The distri-

lated with the ejection velocity for ejecta from Ali Baba (BDAZ, Fig. 29), although there is a slight amount of dynamical 'heating': for spalls, impact speeds are on average about 9% faster than ejection velocities. In any case, for spalls the range of impact speeds is approximately $0.15 < U < 1.3$ km/s, corresponding to 22.7 km $> D_{sg} > 10.4$ km, respectively (Note that at an impact speed of 23.2 km/s $D_{sg} = 3.7$ km, hence crater Ali Baba was created in the gravity regime).

2.7. Size distribution of simulated sesquinary craters

As the ejecta re-accrete on Enceladus, presumably they are going to make craters. By assigning to each ejectum a specific size
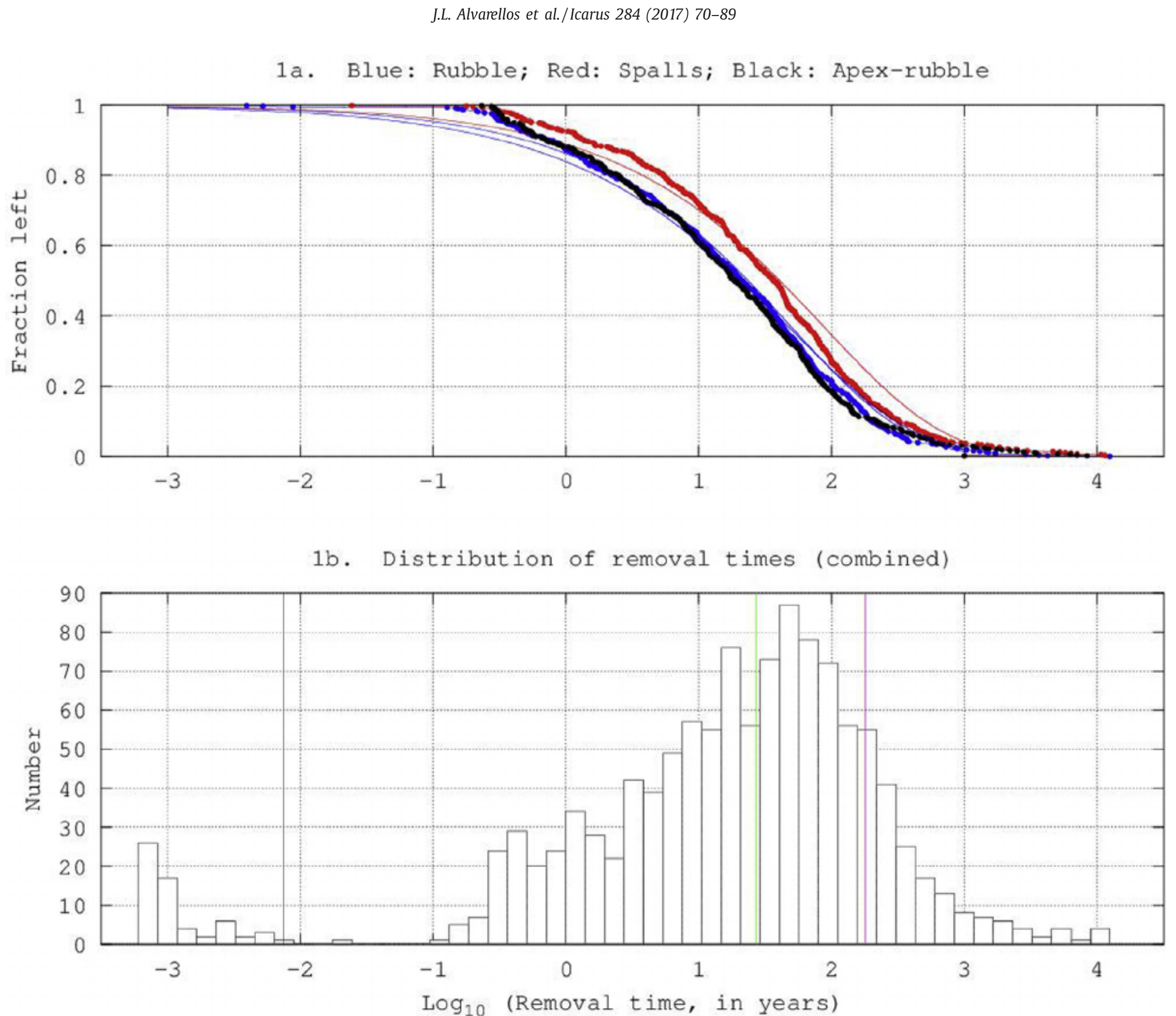
Fig. 1. (a) Removal of the original populations of ejecta escaping Enceladus as a function of time for the simplified system. The removal approximately follows a stretched exponential law (Eq. (10)); the stretched exponential fits are shown as the solid curves. Ali Baba ejecta are shown as red and blue, while ejecta from the apex are shown in black. (b) Distribution of removal times for Ali Baba ejecta returning to Enceladus (apex ejecta not included here); 'Number' refers to the number of particles coming back to Enceladus. The black vertical line represents twice the orbital period of Enceladus (2 × 1.37 = 2.74 days); particles coming back in less time than this are filtered out of the analyses. The median (27 years) and mean (179 years) removal times are shown as the vertical green and magenta lines, respectively. Note that the x-axis is the same in both (a) and (b). (For interpretation of the references to colour in this figure legend, the reader is referred to the web version of this article.)

(the size distribution is determined by Eqs. (8) and (9): the faster the ejection speed, the smaller the size) and knowing its impact speed and incidence angle, per the discussion on Section 2.3, it is straightforward to estimate resulting sesquinary crater sizes. Let us
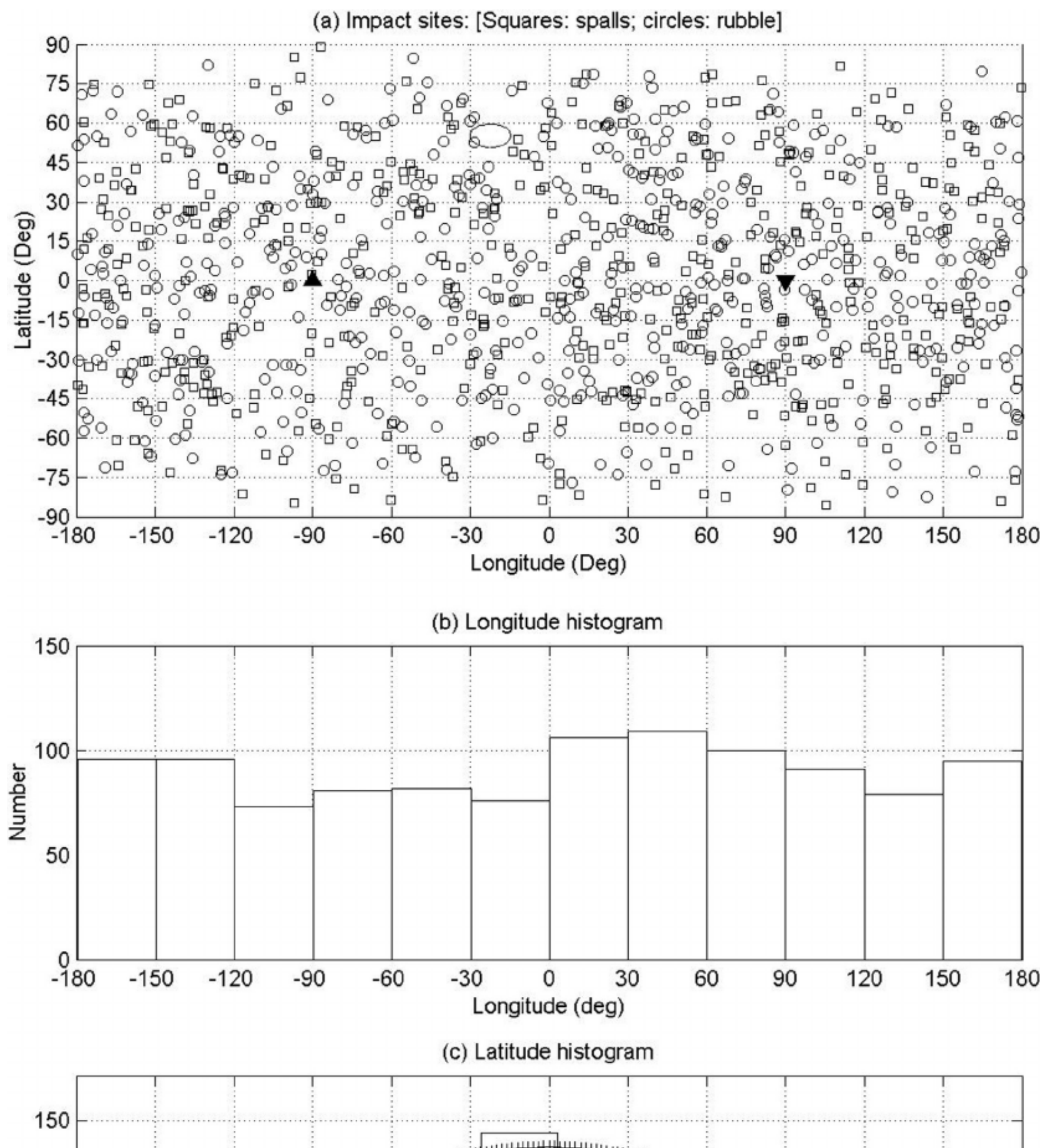
dependent of the regime assumed (not so for the crater sizes as we will see).

Fig. 3 plots the calculated sesquinary crater size-frequency distributions assuming the strength regime. In the top panel (a) we

consider the gravity regime first: if we assume the diameter of an ejectum is given by the Grady–Kipp fragment size (from our calculations, $0.1\ \text{m} < L_{GK} < 0.5\ \text{m}$ depending on the ejection speed, with $\langle L_{GK} \rangle = 0.3\ \text{m}$ for the Ali Baba impact), the average crater diameter is about 9 m. Assuming that the diameter of an ejectum is given by the spall-plate thickness ($4\ \text{m} < Z_s < 27\ \text{m}$, with $\langle Z_s \rangle = 16\ \text{m}$), we obtain larger craters averaging 180 m in diameter. Finally, if we assume that the tabular spall-plates do not break up at launch, and have characteristic diameter given by the mean spall dimension $\langle L_s \rangle = \langle (6 l_s w Z_s / \pi)^{1/3} \rangle = 247\ \text{m}$ (the range is $54\ \text{m} < L_s < 434\ \text{m}$), where l_s and w are the other spall block dimensions (Melosh, 1984), then we find the average crater diameter to be 1500 m. Since all of these crater diameter estimates are smaller than the estimates for D_{sg} we obtained in the last section, we conclude that sesquinary craters must be created in the strength regime. Note that the **ejecta** sizes computed above are in-

assume that the diameter of an ejectum is given by $\langle L_{GK} \rangle$, with an average crater diameter of 1 m. In the middle panel (b) we assume that the diameter of an ejectum is given by $\langle Z_s \rangle$; in this case, the average crater diameter is larger, at about 65 m. Finally in the bottom panel (panel c) we assume that the characteristic diameter is given by the mean spall dimension $\langle L_s \rangle$; then we find the average crater diameters equal to 980 m (largest diameter at 1.9 km). Although the above analyses were done for the spalls case, the rubble ejecta simulation gives very similar results (where instead of Z_s we used l_r given by Eq. (A-12) in AZDH). Note also that all crater diameters are smaller than the simple-to-complex transition diameter ($D_c = 15$ km; Table 1); hence we expect these sesquinary craters to have a simple bowl-shape.

Singer et al. (2013) investigated the size-velocity distribution of ejecta fragments from craters on Europa (Tyre and Pwyll) and Ganymede (Gilgamesh and Achelous). By mapping secondary crater

(a) Impact sites: [Squares: spalls; circles: rubble]
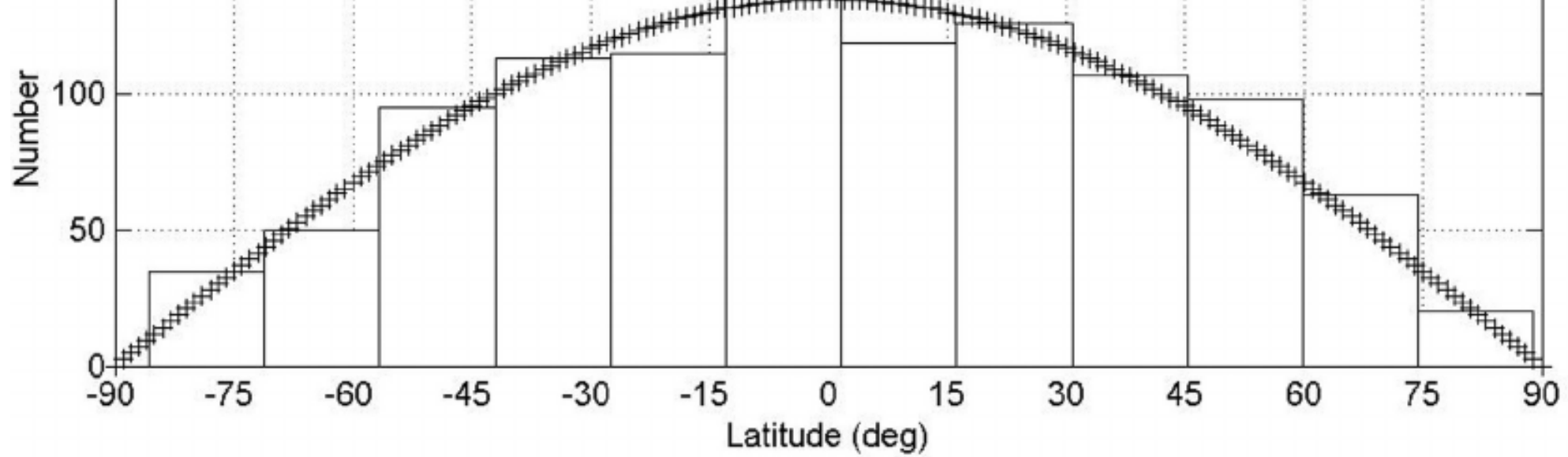
(b) Longitude histogram

(c) Latitude histogram

Fig. 2. (a) Simulated impact sites for the Enceladus ejecta which came back after spending time orbiting Saturn (simplified system). The sub-Saturn point is at (0,0). Squares represent spalls, while circles represent rubble particles. The upward-pointing triangle represents the apex of motion, while the downward-pointing triangle represents the antapex. The oval centered at −22° longitude, 55° latitude represents the outline of crater Ali Baba. (b) Combined distribution (spalls and rubble; simplified system) of impact sites with longitude and (c) latitude; there is no strong preference in the longitudinal distribution of impact sites. The plus signs represent a random distribution of latitude.
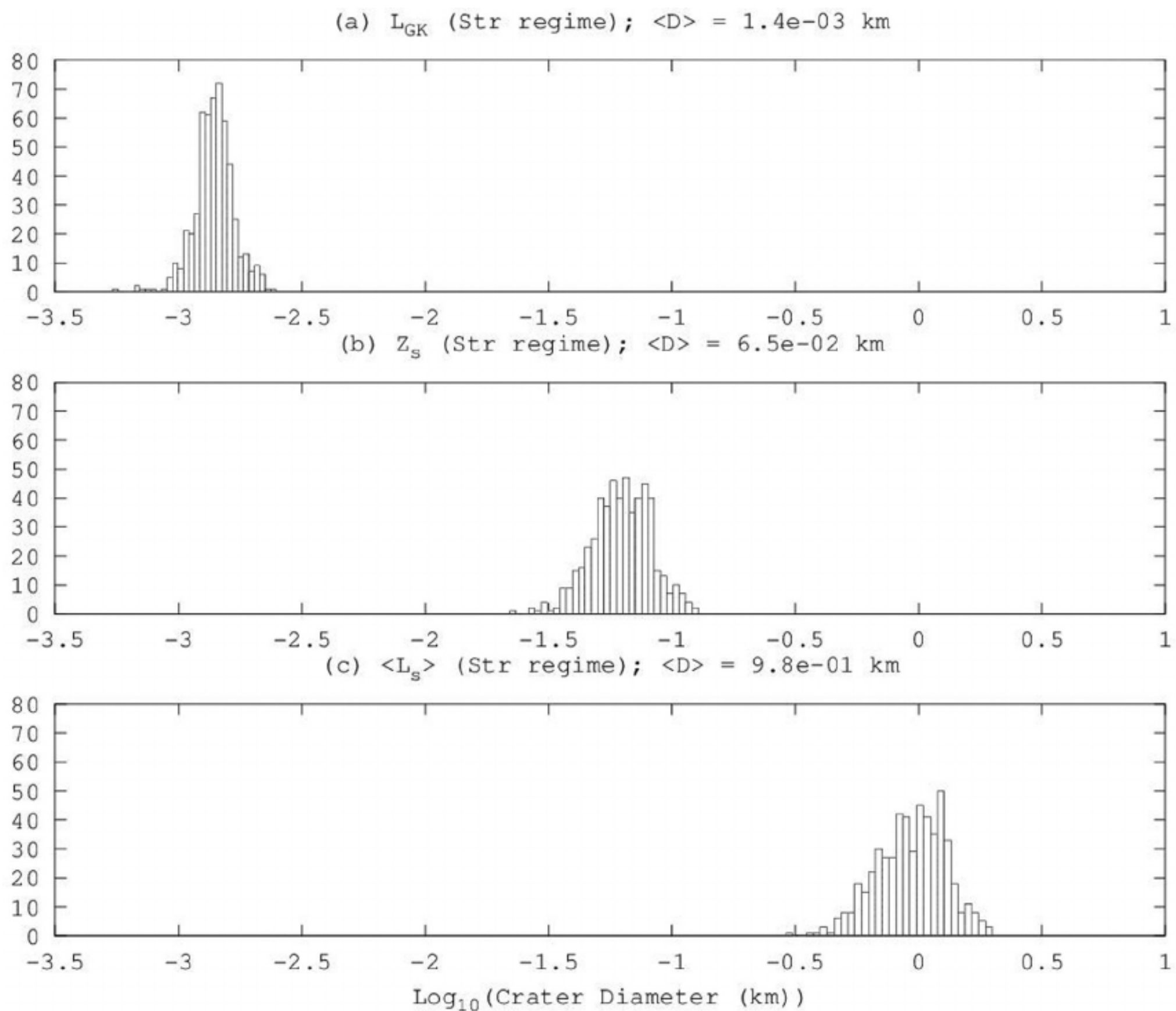
Fig. 3. Size-frequency distribution (SFDs) of simulated sesquinary craters on Enceladus (simplified system). These represent craters made by spall ejecta from Ali Baba that rain back onto Enceladus; impact speeds and incident angles are used to compute sesquinary crater sizes assuming the strength regime. (a) Sesquinary crater size distribution assuming the ejecta size is given by the Grady–Kipp fragment size ($\langle L_{GK} \rangle = 0.3$ m). (b) Size distribution made by assuming the ejecta size is given by the spall-plate thickness ($\langle Z_s \rangle = 16$ m).(c) Crater size distribution made by assuming the ejecta size is given by the mean spall diameter ($\langle L_s \rangle = 247$ m). Results are similar for the rubble simulation; see text for details.

fields, they obtain relationships between the ejecta fragment sizes   Enceladus, while anything traveling faster would be able to escape,

and observed secondary crater diameters. In addition, by characterizing the upper envelope (quantile regression analysis to the 99th percentile) of the ejecta size-velocity distribution derived from secondary craters, they obtain power laws for the largest fragment size d_{fmax} at a given ejection velocity. By scaling to the final, observed crater diameter they obtain a 'master' power law $d_{fmax} = 19.9Dv_{ej}^{-1.17\pm0.06}$ (where v_{ej} is in m/s) applicable to Ganymede and Europa; the caveat, however, is that the data from Pwyll do not quite fit into this law. Singer et al. (2013) obtain

$$\frac{d_{fmax}}{R} \propto \left(\frac{\rho_t gR}{Y}\right)^{-1/3} \left(\frac{v_{ej}}{\sqrt{gR}}\right)^{-1.2} \quad (12)$$

where they assumed non-porous ice, and the R above is the final crater radius. To get an idea of the correct size of ejected blocks, we scale the coefficient of their master power law to Ali Baba (we assumed (a) $Y = \sigma_t$, and we use a strength consistent with that found by Lange and Ahrens (1987) for impact experiments in cold ice, and (b) our baseline crater to be Gilgamesh, on Ganymede) to obtain $d_{fmax} = 4.2Dv_{ej}^{-1.2}$; setting $v_{ej} = v_{esc}^* = 209$ m/s we find that the maximum block size that could have escaped Enceladus from the Ali Baba impact was 271 m in diameter. Anything traveling slower than v_{esc}^* would be larger, but would not be able to escape

but would be smaller. This suggests that the mean spall $\langle L_s \rangle$ diameter approximates the maximum ejectum size. Going back to Fig. 3, we can therefore infer that, while we may see a few sesquinary craters as large as 1.9 km in diameter (the largest sesquinary crater seen in Fig. 3c), the vast majority will be in the meters and tens of meters in diameter, assuming that the vast majority of ejecta capable of making sesquinary craters are of the size scales of $\langle L_{GK} \rangle$ and $\langle Z_s \rangle$. The rubble results do show a slightly higher amount of 'dynamical heating', with impact speeds about 12% faster than ejection speeds, on average; this may be due to their lower launch velocities, which imply stronger scattering.

2.8. Comparison with observations

According to the findings of BDAZ, sesquinary craters should be more common than secondaries on Enceladus, because of its small size. For $v_{min} = 150$ m/s the ratio of ejecta masses available to make sesquinaries to that of secondaries should be $\frac{M_{esc}}{M_{sec}} = 1.8$, while if $v_{min} = 250$ m/s no secondaries should exist. Hence, potentially most, if not all, Enceladean small craters might be sesquinaries.

Observed size-frequency distributions (SFD) of craters are usually presented as 'R-plots', where the 'R' stands for 'relative'.

Table 6
Fate of ejecta from a fictitious 'Apex' crater on Enceladus. Format similar to Table 5.

Target	Rubble (Simp.) N	Rubble (Simp.) Perc.	Rubble (Full) N	Rubble (Full) Perc.
Saturn	0	0	0	0
Rings	0	0	0	0
Mimas	0	0	0	0
Methone	0	0	0	0
Enceladus	529	94.8%	529	94.8%
Tethys	28	5.0%	29	5.2%
Telesto	0	0	0	0
Calypso	0	0	0	0
Dione	0	0	0	0
Helene	–	–	0	0
Polydeuces	–	–	0	0
Rhea	–	–	0	0
Titan	–	–	0	0
Hyperion	–	–	0	0
Iapetus	–	–	0	0
Phoebe	–	–	0	0
Active	1	0.2%	0	0
Escape (P_0)	558	100%	558	100%

Parameter	τ (yrs)	β	τ (yrs)	β
Value	47.5	0.450	45.7	0.425
Uncertainty	± 8.8	± 0.131	± 16.5	± 0.222

Such data can be approximated by power-laws of the form $R_v = D^3 dN/dD$ where dN is the number of craters per unit area with diameters bracketed by D and $D + dD$. BDAZ argue that the sesquinary crater contributions to the observed cratering pattern should force the distribution to be steep (i.e., dominated by small craters), but that is not what is observed. BDAZ produced numerous R-plots for different regions of Enceladus and in most, if not all cases, they note that the crater density per unit area decreases at smaller crater diameters. In all of their R-plots, the smallest observed crater diameters are approximately 300 m or so; as we've shown above, unless sesquinary craters are produced by intact spalls (980 m crater diameter; Fig. 3c), they will be smaller than this. It is also possible, as BDAZ state, that any large ejecta that make it into orbit about Saturn are in such a fragile state that many repeated close encounters with Enceladus tidally disrupt the

An interesting byproduct of this simulation is that we found one particle in the simplified system run which managed to survive 19,000 years and which, upon further investigation, lasted at least 10^6 years in orbit about Saturn between Enceladus and Tethys (see Fig. 4). Except for the first 150,000 years, where the semi-major axis varied in a somewhat chaotic manner and where it suffered a few close approaches to Enceladus, the semi-major axis hovers very steadily around 256,700 km, close to a 9:10 resonance with Enceladus and protected from close approaches to both Enceladus and Tethys. Note that there are no known moonlets between Enceladus and Tethys. However, there are at least three currently known small satellites orbiting between Mimas and Enceladus: Methone, Anthe and Pallene (the Alkyonides group), the last of which is the largest at about 5 km in diameter. In addition, there exists another recently discovered moonlet interior to Mimas, namely Aegaeon; it is embedded in and may contribute material to Saturn's G ring. These moonlets might be related to large impacts on one of the classical, inner icy satellites. No such long-term survivors were found in the full system run.

3. Ejecta from Dione

For ejecta from Dione we chose Aeneas as the source crater. This is a $D = 161$ km diameter ancient crater; its interior is peppered with smaller, newer craters. Like Ali Baba, it is located on the Saturn-facing hemisphere (Table 2). Using Eqs. (1) and (2), and assuming the same impactor and target densities as before and an incidence angle of 45°, we estimate that the comet that created Aeneas hit Dione at 20.4 km/s and its diameter was 10.6 km; its mass was $m_i = 3.7 \times 10^{14}$ kg. The classical escape speed of Dione is $v_{esc} = 520$ m/s, while the modified escape speed is $v_{esc}^* = 0.917v_{esc} = 467$ m/s (assuming an ejection angle of 45°). Following the work done in Section 2.2, we compute the total ejected mass and the amount that escapes Dione; the latter quantity is about $0.7m_i$. To see why it should be so different from the Ali Baba result, note that Eq. (4) for the escaped mass can be expressed as

$$M_{esc} \propto \left(\frac{U^2}{R_m^2 \rho_m}\right)^{0.69} m_i \quad (13)$$

weakly-bound fragments into even smaller pieces, and by the time they actually hit their source moon, the craters they make are even smaller than those in Fig. 3. This might explain the shallow distribution of observed, small craters.

2.9. Ejecta from the apex

In an additional numerical experiment, a fictitious small comet strikes Enceladus at latitude zero and longitude -90° E (i.e., at the apex) with a speed of 27 km/s. We assumed the rubble ejection model, with target and comet densities as before. Initial conditions for the massive moons are the same as in our previous Enceladus runs. After integrating the system forward in time, we again find that the ejecta particle population decays as a stretched exponential. The fates of the particles are similar to our previous runs; however, a larger percentage of ejecta reached Tethys (approximately 5%). In general, the semi-major axes of escaping particles ejected from the apex of motion are expected to be larger than those ejected from anywhere else [1]. Therefore we expect that, everything else being equal, more particles ejected from the apex of Enceladus will reach Tethys than those ejected elsewhere, which indeed is what we observe. Results are summarized in Table 6.

_____

[1] Conversely, semi-major axes of particles ejected from the antapex are expected to be *smaller* than those ejected from anywhere else.

where $\hat{\rho}_m$ is the moon's bulk density (for simplicity we assumed $v^*_{esc} = v_{esc})^2$. Plugging in numbers from Tables 1 and 2 we see that in terms of m_i only about 1/3 as much mass as the Ali Baba impact event escapes Dione. However, because the masses of the impactors are not the same, in absolute terms much more mass escapes (two orders of magnitude more, in fact) from the Aeneas impact event than from the Ali Baba one, i.e., compare Tables 4 and 7.

As in the case of the much smaller Ali Baba crater, the bulk of the ejected mass ends up in the ejecta blanket. However, unlike the Ali Baba case, a larger fraction (between 0.6 and 1.6% of the total ejected mass, depending on which value of v_{min} we choose) goes into making secondary craters; see Table 6. BDAZ indicated that Dione, like Tethys and Rhea, is massive enough that it is expected to show an appreciable population of secondary craters. Schenk et al. (2015) provide evidence for secondary craters on Tethys and Rhea.

3.1. Dione ejecta: results

The fraction of mass that escapes Dione from the Aeneas impact event is about 0.4%. Following the discussion of Section 2.4,

_____

[2] This relation says nothing about the probability of getting hit by a comet, of course; however, for objects that do get hit, the most vulnerable ones are small, low-density objects where the impact velocity is high, i.e., those located deep in a potential well.
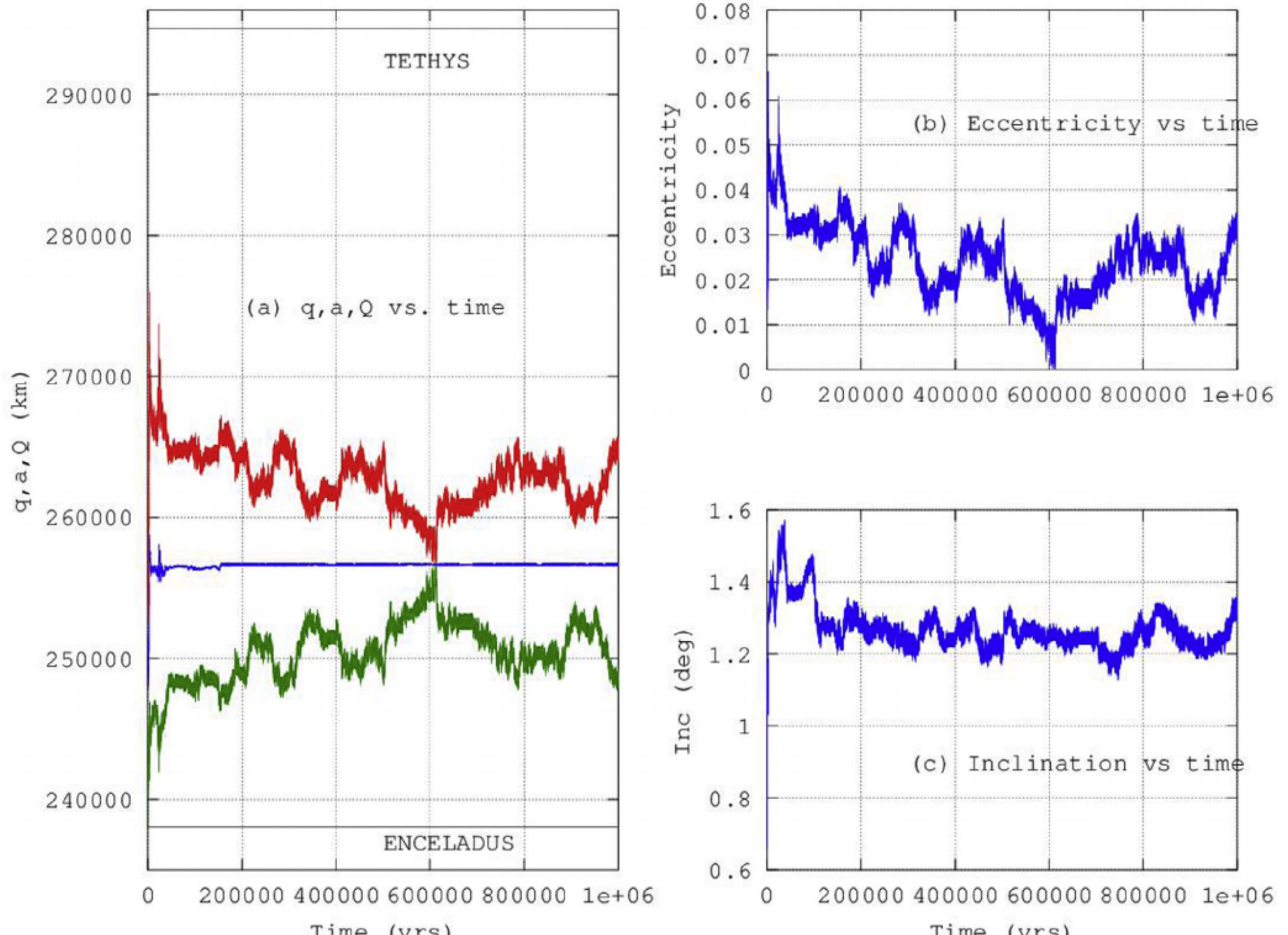
Fig. 4. (a) Semi-major axis a, periapse $q = a[1 - e]$ and apoapse $Q = a[1 + e]$ of a long-lasting (10^6 years) particle ejected from a fictitious crater at the apex of Enceladus. Other than irregular behavior during the first 150,000 years, this particle settled thereafter into a 9:10 near-resonance with Enceladus, where it was not only protected from further close encounters with it, but also close encounters with Tethys. Semi-major axes of Enceladus and Tethys are indicated. (b) Behavior of the eccentricity, which varies chaotically between 0.0001 and 0.0664, with a mean value of 0.0240. Note that it is this behavior that controls q and Q. (c) Behavior of the inclination.

Table 7

The total and fractional masses for crater Aeneas (on Dione) and resulting ejecta. The total mass ejected is $M_{tot} = 6.215 \times 10^{16}$ kg. Format similar to Table 4. Compare with Table 2 of BDAZ.

v_{min} (m/s)	M_{eb} (kg)	f_{eb}	M_{sec} (kg)	f_{sec}	M_{esc} (kg)	f_{esc}
150	6.090×10^{16}	0.980	9.837×10^{14}	0.016	2.587×10^{14}	0.004
250	6.153×10^{16}	0.990	3.552×10^{14}	0.006	2.587×10^{14}	0.004

for Dione spall ejecta we obtain $v_{esc}^* < v_{ej} < 2.39$ km/s while for rubble ejecta we obtain $v_{esc}^* < v_{ej} < 1.98$ km/s. As before, we simulate the dynamical evolution of escaping ejecta from this crater using Swift, and using a simplified and a full system. For the former we include the gravitational perturbations of Enceladus, Tethys, Dione itself and its two Trojan companions Helene and Polydeuces, as well as Rhea and giant Titan. For the simplified system, we did not include Mimas' gravitational perturbations directly; instead we added its mass to Saturn's, with the appropriate shift in center of mass. Methone's mass is so small that we ignored it for these simulations; we did the same for the Trojan companions of Tethys. For the full system we used the same massive bodies as in Section 2 (including the Sun).

Table 8 summarizes our findings. As expected, most escaping ejecta (between 80 and 91%, depending on the model) come back

to Dione, but significant fractions reached Tethys (between 1.4 and 1.9%) and Rhea (between 7.0 and 19.0%). No particles struck either of Dione's Trojan companions, nor Saturn's rings. There were no survivors in any of these 10^5 year runs; the longest-lived particle was removed after 46,526 years (in the full system, spalls run). Table 8 shows that spall and rubble results are more dissimilar than in the Enceladus case: rubble ejecta from Dione are more likely than spalls to come back to the source.

The Dione results are comparable to the results found for ejecta from Tethys: in AZDH (see Tables 6 and 7 therein) we simulated escaping ejecta from craters Odysseus (near the leading side) and Penelope (near the trailing side). Depending on the crater and the initial conditions assumed, between 81.5 and 95.9% of ejecta came back to Tethys; ejecta from the leading side that did not come back home reached Dione itself (as much as 16%) and a smaller fraction hit Rhea. Conversely, ejecta from the trailing side that did not return preferentially reached Enceladus (as much as 5.8%). Big impacts provide a mechanism for exchanging mass among moons.

Curve fitting shows that again the stretched exponential decay (Eq. (10)) fits the actual population decays best; we list these fit parameters at the bottom of Table 8. As in Section 2, in what follows we refer to the result of the simplified system (unless

Table 8

Fate of ejecta from crater Aeneas on Dione (simulation time = 10^5 years). Format similar to Table 5.

Target	Simplified system				Full system			
	Rubble		Spalls		Rubble		Spalls	
	N	Perc.	N	Perc.	N	Perc.	N	Perc.
Saturn	0	0	0	0	0	0	0	0
Rings	0	0	0	0	0	0	0	0
Mimas	–	–	–	–	0	0	0	0
Methone	–	–	–	–	0	0	0	0
Enceladus	0	0	0	0	0	0	0	0
Tethys	11	1.9%	10	1.7%	11	1.9%	8	1.4%
Telesto	–	–	–	–	0	0	0	0
Calypso	–	–	–	–	0	0	0	0
Dione	521	89.4%	463	80.1%	531	91.1%	460	79.6%
Helene	0	0	0	0	0	0	0	0
Polydeuces	0	0	0	0	0	0	0	0
Rhea	51	8.7%	105	18.2%	41	7.0%	110	19.0%
Titan	0	0	0	0	0	0	0	0
Hyperion	–	–	–	–	0	0	0	0
Iapetus	–	–	–	–	0	0	0	0
Phoebe	–	–	–	–	0	0	0	0
Active	0	0	0	0	0	0	0	0
Escape (P_0)	583	100%	578	100%	583	100%	578	100%

Parameter	τ (yrs)	β	τ (yrs)	β	τ (yrs)	β	τ (yrs)	β
Value	88.7	0.512	143.9	0.518	91.8	0.506	154.7	0.491
Uncertainty	± 12.5	± 0.106	± 46.8	± 0.205	± 12.5	± 0.102	± 56.8	± 0.217

otherwise stated). The decay curves are shown in Fig. 5. The mean removal time for escaping Dione particles coming back is 181 years, while the median removal time is 39 years. Meanwhile there were 21 ejecta particles in total which reached Tethys: the mean and median times to get from Dione to Tethys were 315 and 142 years respectively, while the minimum time was 53 years. In addition, there were 156 particles which reached Rhea: curiously,

3.2. Size distribution of simulated sesquinary craters

The impact speeds of the ejecta returning to Dione are shown in Fig. 7. Impact speeds are approximately linearly correlated to ejection speeds, as was the case for the Ali Baba ejecta. There is a slight amount of dynamical 'heating' as well, as evidenced by the fact that the slopes are not unity: for spalls ejecta the slope

the minimum time to get there was only 1.5 years, while the mean and median times were 620 and 301 years, respectively.

Similarly to (Zahnle et al., 2001; Leliwa-Kopystynski et al., 2011, Fig. 2; LKBW henceforth) quantified the level of longitudinal cratering asymmetry by using the ratio of the number of craters on the antapex to that on the apex of motion; unlike Zahnle et al. 2001, however, they considered craters only in the equatorial region (± 5° in the case of Dione) and called this parameter the 'Equatorial Measure of Cratering Asymmetry', or EMCA. They measured and plotted the longitudinal distribution of craters observed on the surface of Dione for four different size ranges: $0.74 < D < 2.74$ km; $2.74 < D < 5.15$ km; $5.15 < D < 7.35$ km; and $7.35 < D < 9.56$ km. They found a weak dependence on longitude (EMCA = 1.6), with a maximum crater density on the anti-Saturn hemisphere.

Fig. 6 a shows the latitude and longitude of impact sites for the returning Aeneas ejecta. As in the case of Ali Baba ejecta, because Aeneas is nowhere near either the apex or antapex points of Dione, the sesquinary crater locations appear random. However, Fig. 6b, which shows the sesquinary crater longitude distribution, shows a slight preference for the trailing hemisphere. Morrison et al. (1986) note that Dione has a higher albedo on the leading hemisphere. Fig. 6c shows the latitude distribution: more nearer the equator, fewer towards the poles, as expected.

Assuming that most, if not all, small craters on Dione are sesquinary, it is not surprising that there is not much correlation between the measured distribution of small craters and the distribution from our simulation. We numerically estimated the sesquinary distribution arising solely from one source crater, while Dione has many large craters besides Aeneas, such as Sabinus, Turnus, Dido, Amata, etc. We shall now estimate the size of these sesquinary craters, for which we need estimates of the ejecta masses and impact speeds.

is 1.04, while for rubble the slope is 1.09. This is likely caused by the gravitational interactions of the particles with Dione and other moons while orbiting Saturn. The impact speeds of the returning fragments range from $0.5 < U < 3.8$ km/s, with corresponding $7.2 > D_{sg} > 3.5$ km.

As before, let us estimate sesquinary crater sizes in the gravity regime first. If we assume that the diameter of an ejectum is given by the Grady–Kipp fragment size ($\langle L_{GK} \rangle = 1.7$ m for the Aeneas impact), the resulting crater diameter is about 27 m. Assuming that the diameter of an ejectum is given by the spall-plate thickness ($\langle Z_s \rangle = 51$ m), the average crater diameter is larger, at about 386 m. Therefore so far, sesquinary craters made on Dione by ejecta of these sizes are unambiguously made in the strength regime. Finally, if we assume that the tabular spall-plates have a characteristic diameter given by the mean spall dimension ($\langle L_s \rangle = 707$ m), then we find the average crater diameters to be as large as 3 km in the gravity regime. However, we find that the largest sesquinary crater in this regime is about 5 km in diameter; hence it is possible that, if tabular spall-plates are capable of surviving the ejection, the largest sesquinary craters may have been produced in the gravity regime.

In Fig. 8 we plot crater size-frequency distributions for the spall ejecta in the strength regime. As in Fig. 3, the top panel assumes that the diameter of an ejectum is given by the Grady–Kipp fragment size $\langle L_{GK} \rangle$; the resulting crater diameter is about 7 m (panel a). The middle panel (b) assumes that the diameter of an ejectum is given by the spall-plate thickness $\langle Z_s \rangle$; in this case, the average crater diameter is larger, at about 207 m. In the bottom panel, we assume that the tabular spall-plates have a characteristic diameter given by $\langle L_s \rangle$; then we find the average crater diameters as large as 2.8 km.

Scaling the power law of Singer et al. (2013) to Aeneas, we obtain $d_{fmax} = 8.7 D v_{ej}^{-1.2}$, so that by setting the ejection speed to the

5a. Blue: Rubble; Red: Spalls

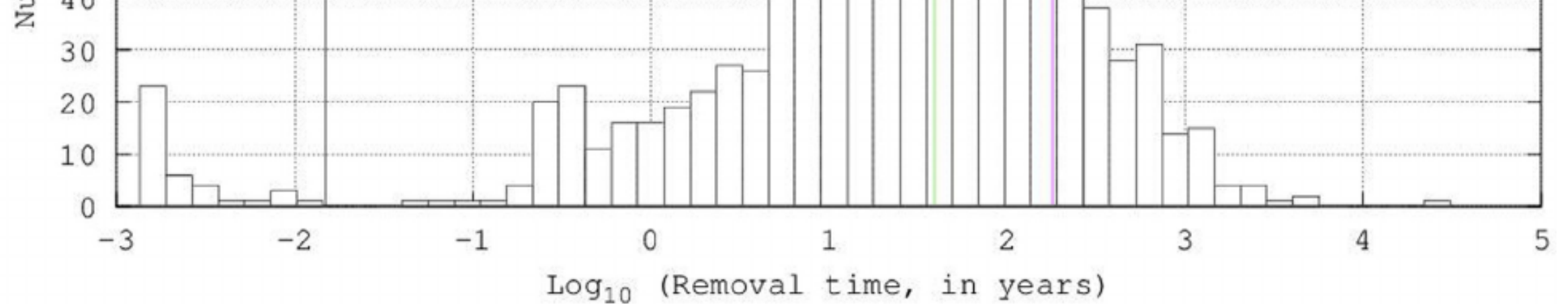5b. Distribution of removal times (combined)
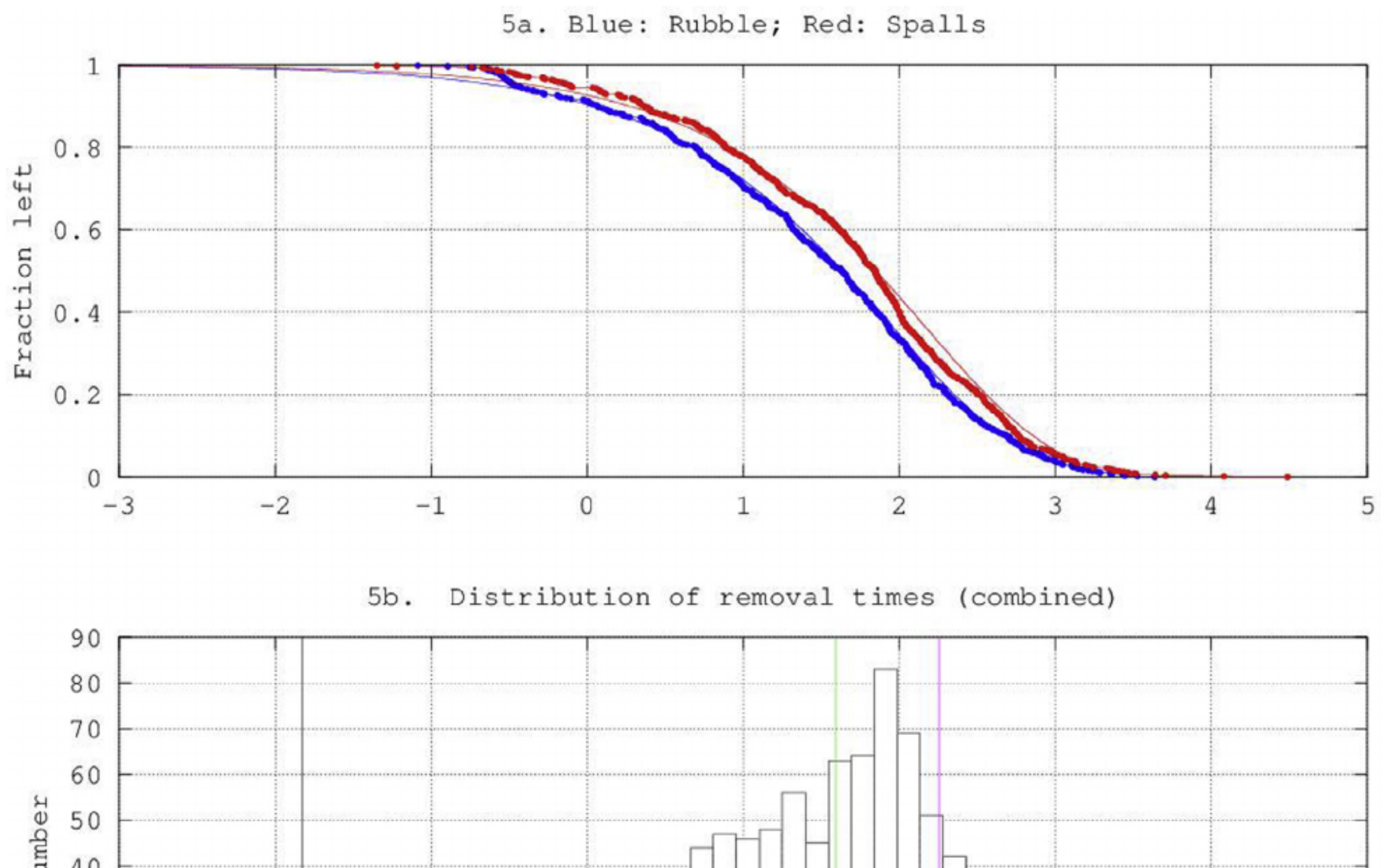
Fig. 5. (a) Removal of the original populations (blue: rubble; red: spalls) of ejecta from Aeneas crater escaping Dione as a function of time (simplified system). The removal approximately follows a stretched exponential law (Eq. (10)); the stretched exponential fits are shown as the solid curves; see Table 7 . (b) Distribution of removal times for ejecta particles coming back to Dione; 'Number' refers to the number of particles coming back to Dione. The black vertical line represents twice the orbital period of Dione ($2 \times 2.74 = 5.48$ days); particles coming back in less time than this are filtered out of the analyses. The median (39 years) and mean (181 years) removal times are shown as the vertical green and magenta lines, respectively. Note that the x-axis is the same in both (a) and (b). (For interpretation of the references to colour in this figure legend, the reader is referred to the web version of this article.)

minimum speed needed to escape Dione (467 m/s), we obtain $d_{fmax} = 877$ m, somewhat larger than the mean spall diameter. As in the previous case, we can conclude that, while it is possible for a sesquinary crater resulting from the Aeneas impact event to be as large as 5 km in diameter (see Fig. 8c), most sesquinary craters will be in the sub-kilometer range. The rubble ejecta simulations give very similar results (where instead of Z_s we used l_r given by Eq. (A-12) in AZDH).

According to BDAZ, Dione should have an abundance of secondary craters. In fact, for $v_{min} = 150$ m/s the ratio of the masses available to make sesquinaries to that of secondaries should be $\frac{M_{esc}}{M_{sec}} = 0.25$, while if $v_{min} = 250$ m/s the ratio is 0.67. In either case, and assuming that sesquinary craters exist on Dione, it might be difficult to distinguish them from secondaries.

4. Ejecta from Mimas (revisited)

In AZDH we investigated the fate of escaping ejecta from the giant impact basin Herschel on Mimas ($D = 130$ km, whereas the diameter of Mimas itself is 394 km). We showed that this crater was plausibly created by a 4.6 km diameter heliocentric comet traveling at 32 km/s ($m_i = 3.06 \times 10^{13}$ kg). Our findings were that most ejecta (between 93.4% and 99.6%, depending on the ejection mechanism adopted) are re-accreted by Mimas itself, and that most of these hit on the trailing side. This is expected, since Herschel is located almost exactly on the apex of Mimas; in Fig. 9 we reproduce Fig. 12 of AZDH, but in the longitude range $-180°$ to $180°$ (rather than $0°$ to $360°$). Note that Horedt and Neukum (1984) noticed an enhancement in crater density towards Mimas' antapex in Voyager data; however they do not mention crater sizes. The few particles not re-accreted by Mimas either survived the 1000 year integration or reached Enceladus. The stretched exponential decay was found to be the best fit to the decay curves, which are shown in Fig. 5 of Dobrovolskis et al. (2007). The accretion rate is rather rapid: Dobrovolskis et al. (2007) found that for the rubble ejecta $\tau = 64$ years and $\beta = 0.54$, while for spall ejecta $\tau = 75$ years and $\beta = 0.62$.

Given the updated findings of LKBW and the work of BDAZ, we revisit the potential of Mimas ejecta to make sesquinary craters. The total ejected mass is $M_{tot} = 3.5 \times 10^{16}$ kg. The escap-

(a) Impact sites: [Squares: spalls; circles: rubble]
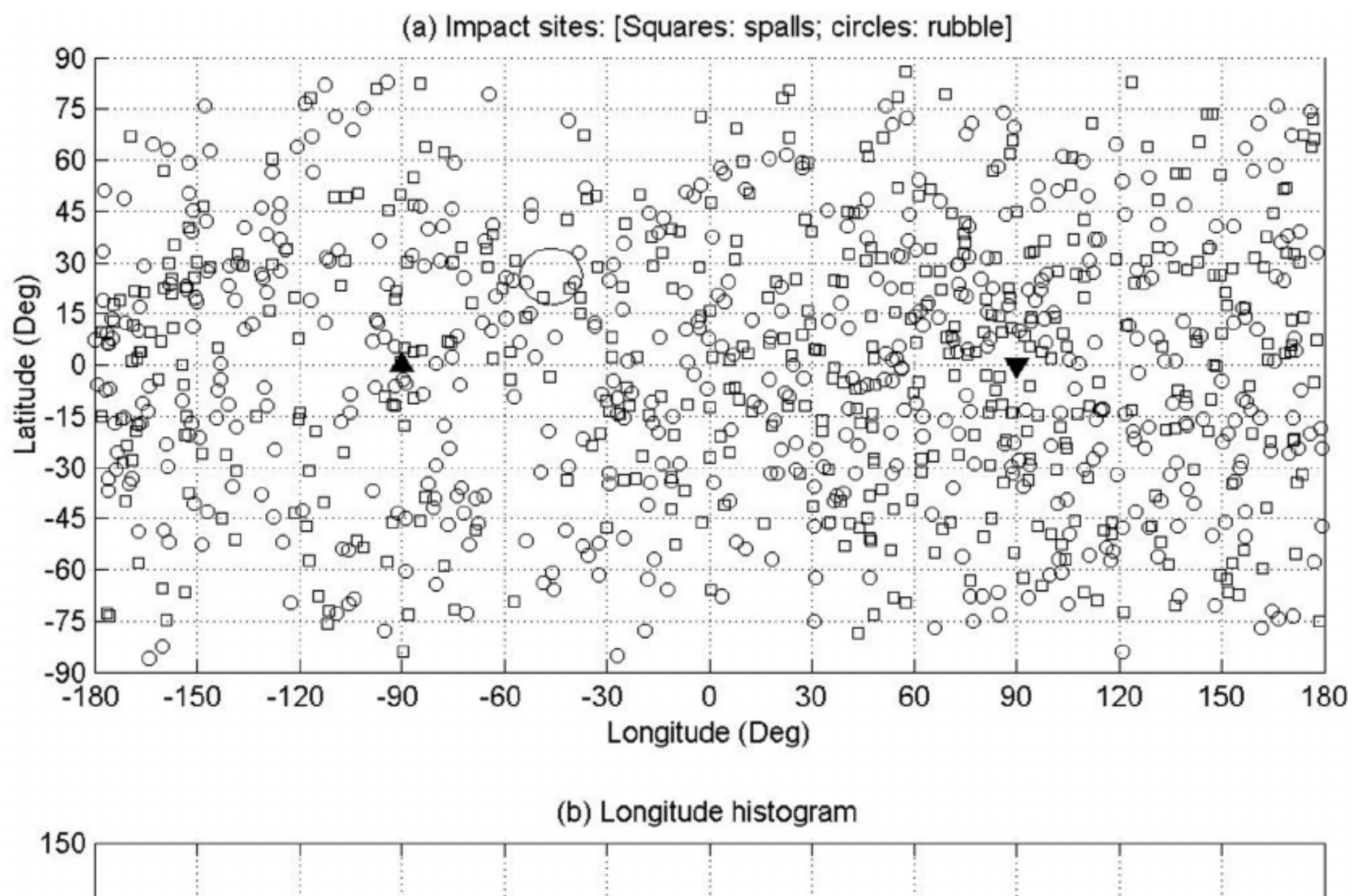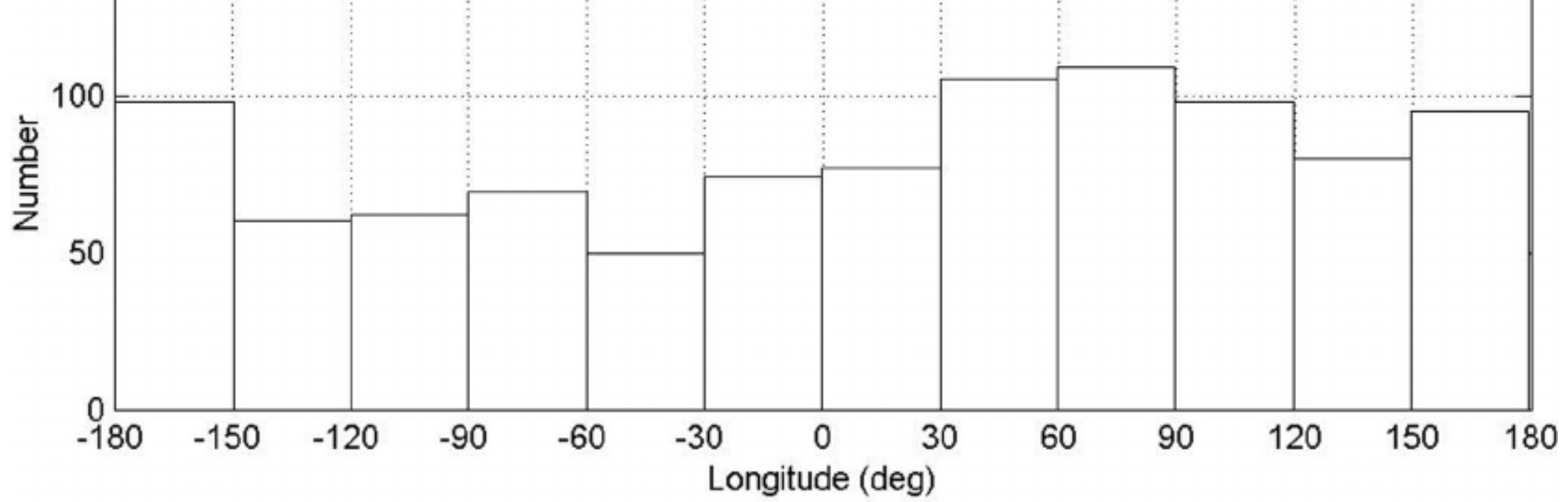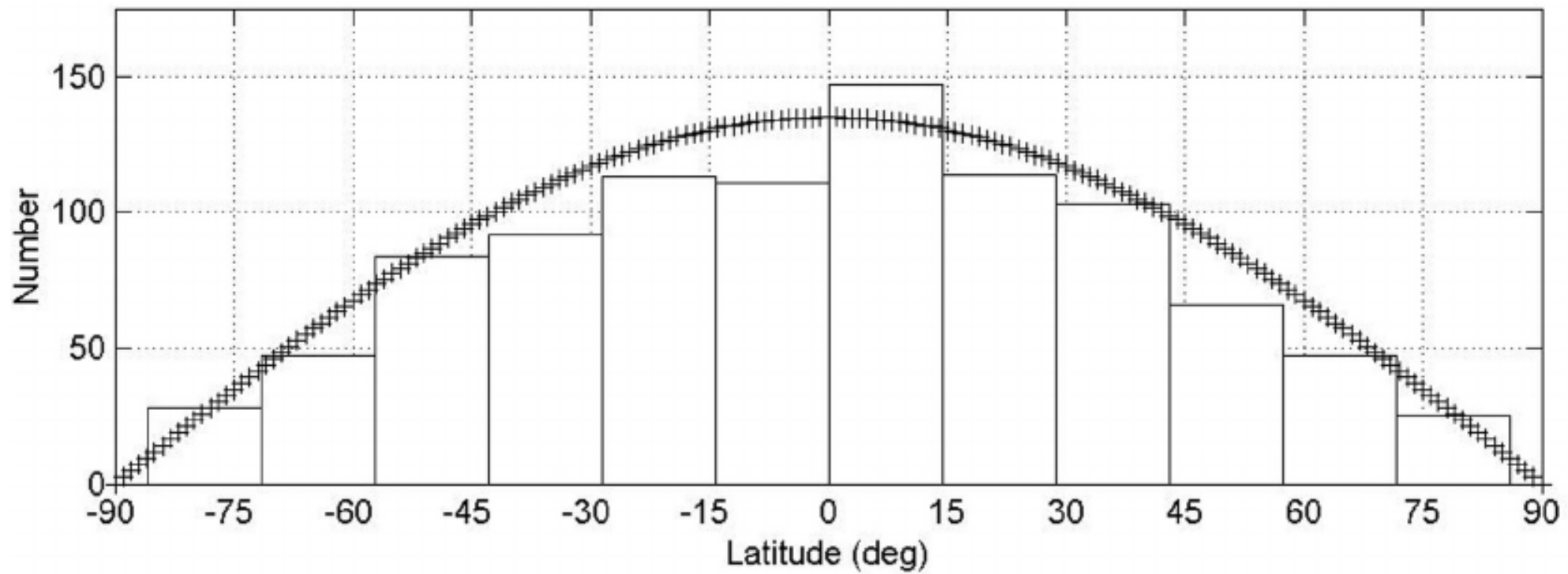
(b) Longitude histogram

Fig. 6. (a) Simulated impact sites for the Dione ejecta which came back after spending time orbiting Saturn (simplified system). Format similar to Fig. 2. The oval centered at −46° longitude, 26° latitude represents the outline of crater Aeneas. (b) Combined distribution (spalls and rubble; simplified system) of impact sites with longitude and (c) latitude; there is a slight preference for the antapex region in the longitudinal distribution of impact sites. The plus signs represent a random distribution of latitude.

ing mass is given by Eq. (4), with $v^*_{esc} = 0.82 v_{esc} = 130$ m/s so that $M_{esc} = 2.2 \times 10^{14}$ kg, or approximately $7.3 m_i$. The range of speeds for Herschel ejecta is as follows: for spall ejecta we obtain $v^*_{esc} < v_{ej} < 1.02$ km/s while for rubble ejecta we obtain $v^*_{esc} < v_{ej} < 0.61$ km/s. Note that v^*_{esc} for Mimas is lower than the lowest

$v_{\min}$ considered (150 m/s), which implies that Mimas should have no secondary craters (BDAZ), a prediction borne out by the latest detailed crater measurements (Robbins et al., 2015). Hence, all ejected mass is partitioned into either the ejecta blanket (the majority), or into escaping mass. This makes Mimas the ideal place to
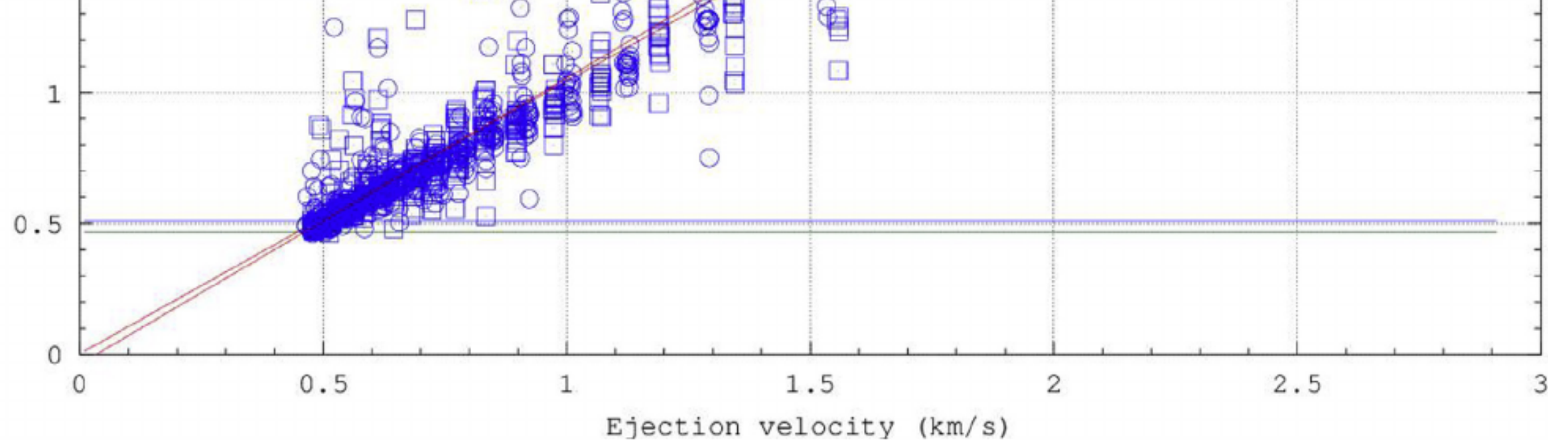
[Square: spalls; circles: rubble]
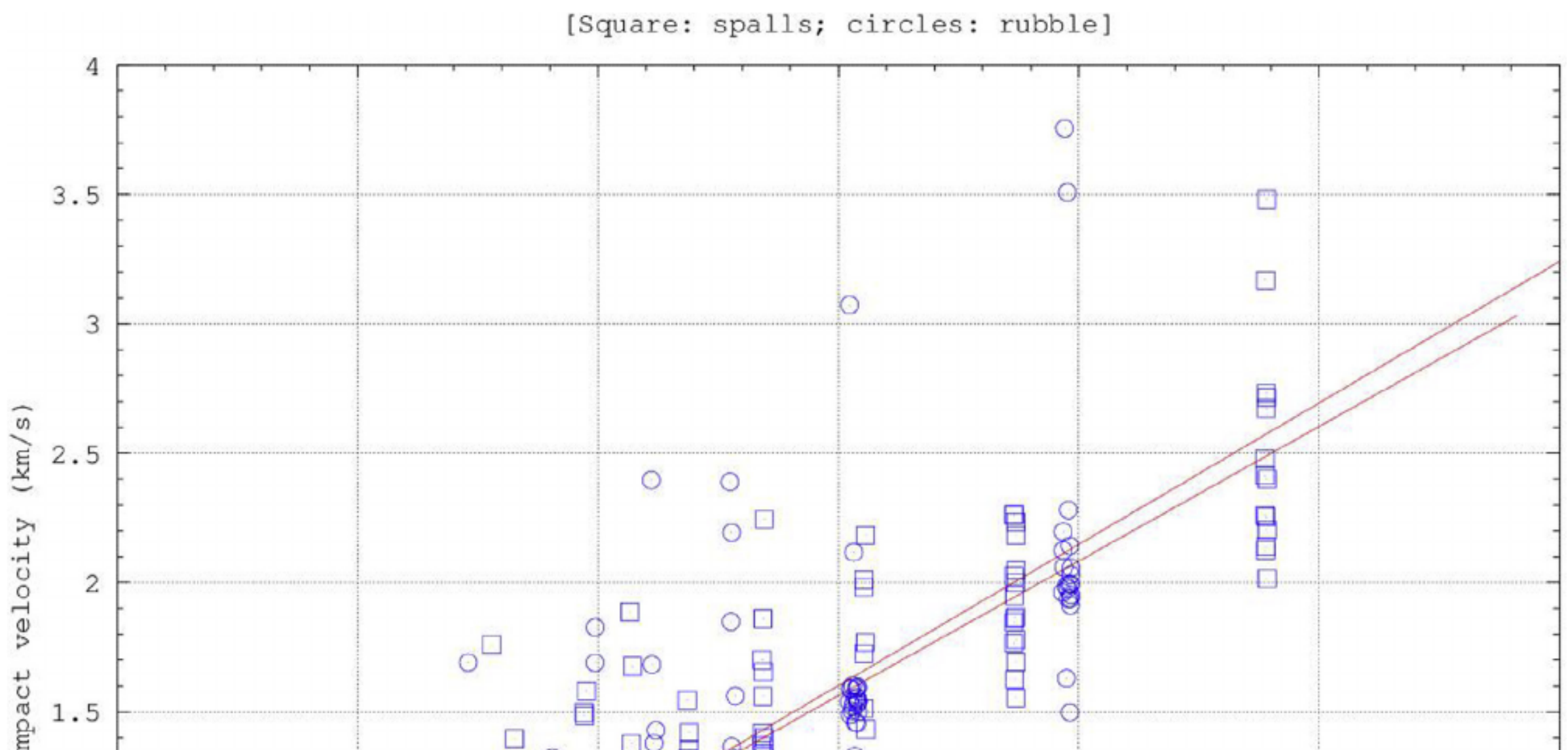
Fig. 7. Impact speed vs. ejection speed for escaping ejecta expelled from crater Aeneas, on Dione (simplified system). The upper horizontal line is the classical escape speed from Dione (520 m/s), while the lower horizontal line represents Dione's modified escape speed (467 m/s; see Eq. (5)). The least-squares fitted line for the spalls ejecta has a slope of 1.04 (squares), while the corresponding slope for the rubble ejecta is 1.09 (circles). As a reminder, the faster particles come from regions closer to the crater's center. Vertical striations are an artifact produced by the quantized way the ejecta were simulated.

Table 9
The total and fractional masses for crater Herschel (on Mimas) and resulting ejecta. The total mass ejected is $M_{tot} = 3.522 \times 10^{16}$ kg. Format similar to Table 4. Note that in the case of Mimas, no ejecta mass is available to make secondary craters, so that both cases are exactly the same.

v_{min} (m/s)	M_{eb} (kg)	f_{eb}	M_{sec} (kg)	f_{sec}	M_{esc} (kg)	f_{esc}
150	3.509×10^{16}	0.994	0.00	0.000	2.232×10^{14}	0.006
250	3.509×10^{16}	0.994	0.00	0.000	2.232×10^{14}	0.006

search for sesquinary craters: if these exist, they should be abundant there. In Table 9 we show the allocation of expelled mass from Herschel; compare with Table 2 of BDAZ.

4.1. Size distribution of simulated sesquinary craters

AZDH estimated sesquinary crater diameters from infalling Herschel ejecta: diameters ranged from ≈ 1 to 6 km; the larger value assumes spall plates surviving the ejection process more or less intact, an unlikely scenario given in Zahnle et al. (2008)'s updated analysis. A plot of the impact speed versus ejection speed for the Mimas data from AZDH is shown in BDAZ (Fig. 29); as was the case of Enceladus and Dione, ejection and reimpact velocities are sim-

ilar, except that low speed ejecta reimpact at speeds a few times higher than the ejection speed.

The range of impact speeds of returning Mimas ejecta from Herschel is $0.1 < U < 1.6$ km/s (AZDH Fig. 13; BDAZ Fig. 29), with corresponding $47.1 > D_{sg} > 17.2$ km (strength to gravity crater diameter transition). First let us estimate sesquinary crater diameters assuming the gravity regime. If the ejecta size is characterized by the Grady–Kipp size ($L_{GK} = 1$ m for the Herschel impact event), the average crater diameter is 24 m. In contrast, if the characteristic ejecta size is given by the spall-plate thickness ($Z_s = 71$ m), the average crater diameter is 726 m. Finally, assuming the fragments survive the ejection process as intact tabular spalls ($\langle L_s \rangle = 1126$ m), the average crater diameter is 6.3 km (AZDH). Scaling the master power law of Singer et al. (2013) to Herschel we obtain $d_{fmax} = 5.8Dv_{ej}^{-1.2}$, and setting $v_{ej} = v_{esc}^* = 130$ m/s we obtain $d_{fmax} = 2191$ m, a factor of two larger than the size scale given by the mean spall diameter. Since estimated crater diameters in the gravity regime are all much smaller than the transition diameters, we conclude that sesquinary craters on Mimas will unambiguously be created in the strength regime.

In Fig. 10 we plot crater size-frequency distributions for the Herschel spall ejecta in the strength regime. In this regime, if the characteristic ejecta fragment size is given by the Grady–Kipp size, the mean crater diameter is 4 m (panel a). On the other hand, if
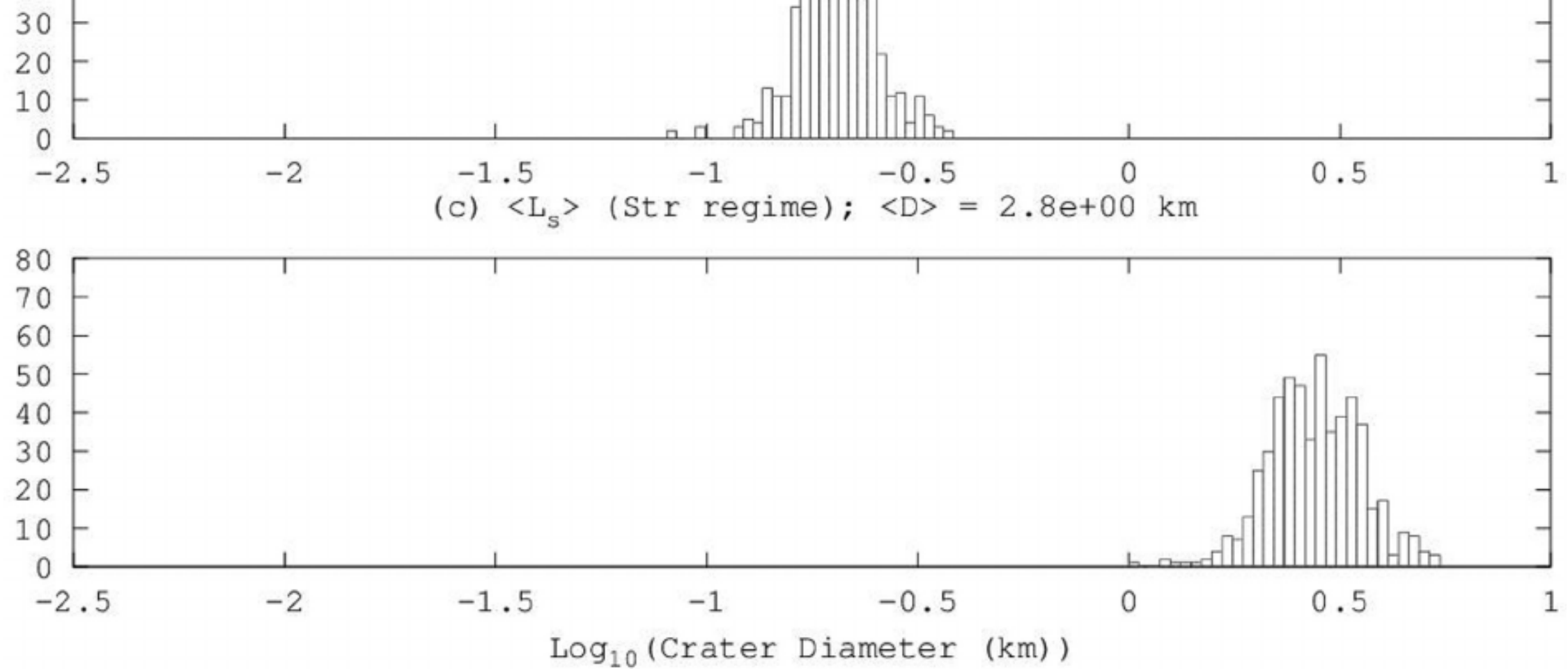
(a) L_{GK} (Str regime); <D> = 7.0e-03 km

(b) Z_s (Str regime); <D> = 2.1e-01 km
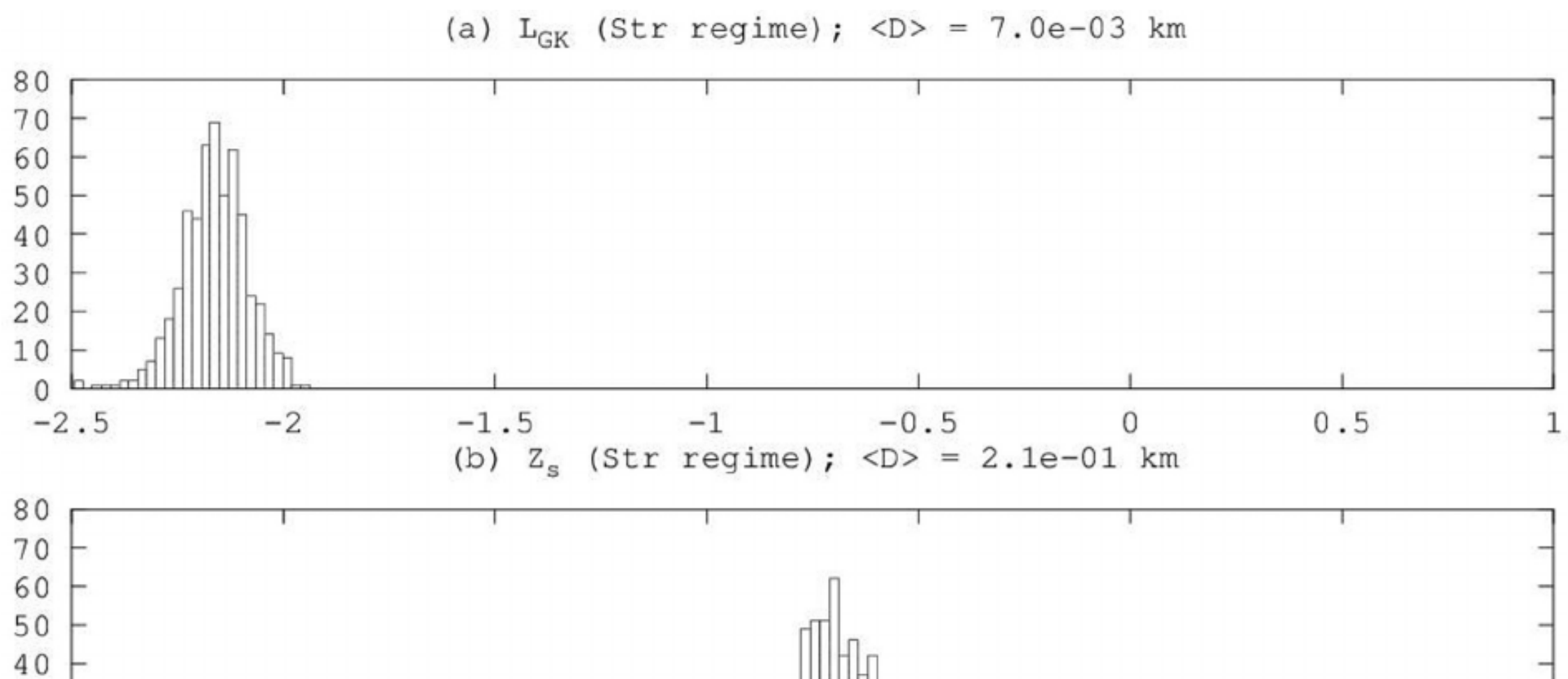
Fig. 8. SFDs of simulated sesquinary craters onto Dione made by spall ejecta from Aeneas in the strength regime (simplified system). Format similar to Fig. 3. It is possible that the largest craters made by intact spalls (panel c) may be created under the gravity regime. Results are similar for the rubble simulation. See text for details.

the characteristic ejecta fragment size is given by the spall-plate thickness, the mean crater diameter is 340 m (panel b). Finally, assuming $\langle L_s \rangle$, the mean crater diameter is 5.4 km (panel c).

Perhaps a plausible way to explain both sets of contradictory observations (R-plots as well as the crater density distributions) is to postulate that during the impact event most, but not all, ejecta fragments are expelled as loosely-held clods. As these ejecta orbit Saturn numerous times, the weakly-bound clumps (perhaps of characteristic size given by $\langle Z_s \rangle$) become disrupted and turn into individual small fragments (with characteristic sizes comparable to L_{GK}), which upon accretion pepper the surface with diminutive craters too small to detect presently (the best images of Mimas currently are just under 100 m/px, that is, the smallest craters we can reliably measure are only about 0.5 km), explaining the observed shallow distribution. At the same time, the small minority of firm ejecta (again, of characteristic size $\langle Z_s \rangle$) that survive more or less intact until their impact on Mimas would explain the observed distributions found by LKBW. Finally, a tiny fraction of ejecta survive as large intact blocks, but the relatively large sesquinary craters that result would be the exception rather than the rule. In other words, the size-frequency distribution of ejecta is modified during the time spent orbiting Saturn such that the mean ejectum size becomes smaller as a function of time.

4.2. Comparison with observations

As in the case of Dione, LKBW measured crater density as a function of longitude (for craters $\pm 30°$ from the equator in the case of Mimas). Unlike the case of Dione, however, there is a strong correlation between crater density and longitude: density is highest near the antapex as predicted by AZDH. Because Herschel so completely dominates over every other Mimantean primary crater, its sesquinary signature should overwhelm that of other primary craters and this may help explain the concordance between the observed and predicted (AZDH) distributions. LKBW measured the value of EMCA on Mimas to be 3.4 (1079 craters), that is, there were 3.4 times more craters at the antapex than at the apex. Furthermore the correlation is stronger at the smaller sizes, which is what would be expected if these (small) craters had originated from re-accreted Herschel ejecta. The crater size bins LKBW considered were $1.15 < D < 4.23$ km (EMCA = 3.5); $4.23 < D < 7.31$ km (EMCA=2.0); $7.31 < D < 10.39$ km (EMCA = 1.2); and $10.39 < D < 13.46$ km (no EMCA value reported). However, R-plots of craters on Herschel show that the relative crater density decreases with decreasing diameter.

In addition, we have made our own measurements of craters on Mimas. We have used the latest coordinate system for Mimas
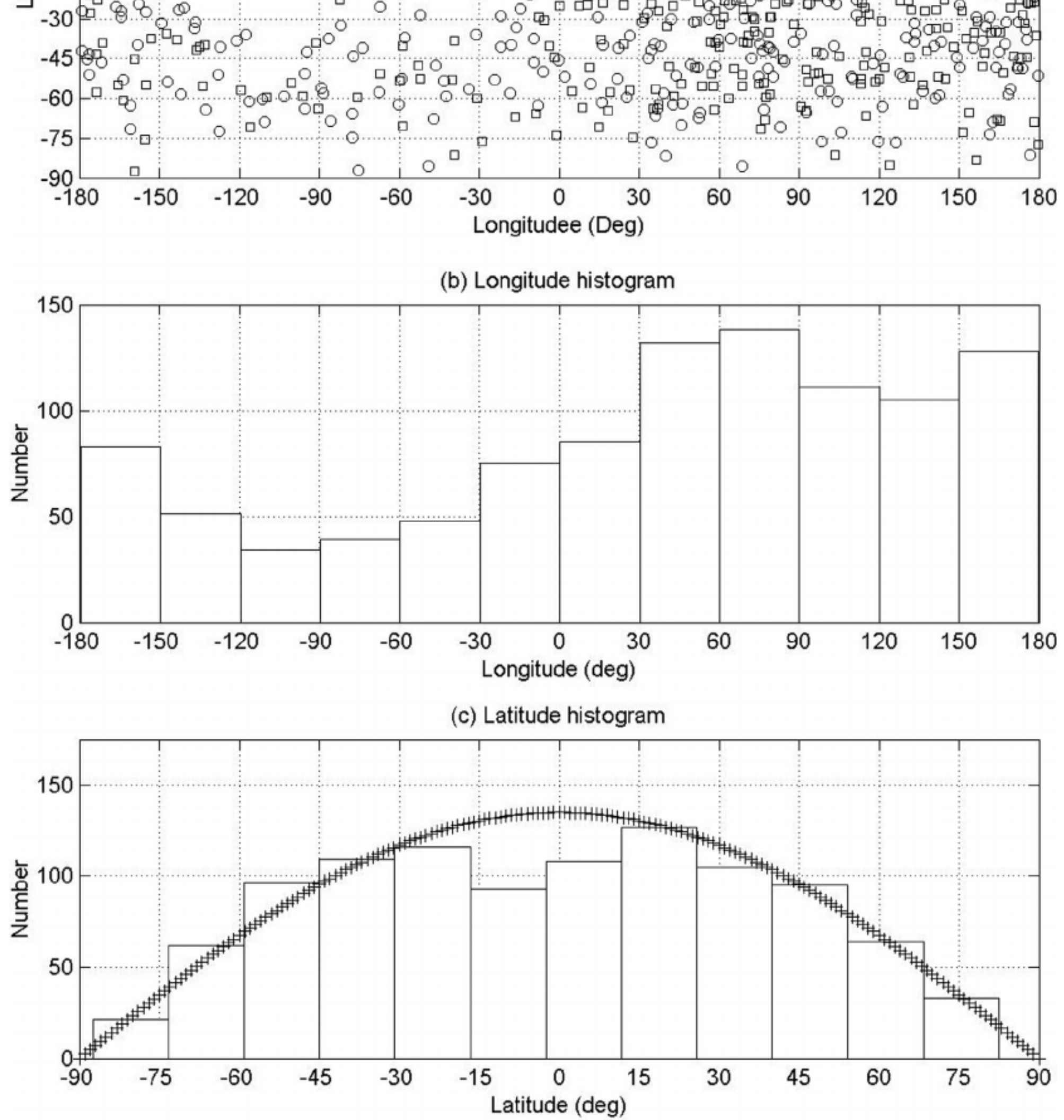
(a) Impact sites

(b) Longitude histogram

(c) Latitude histogram
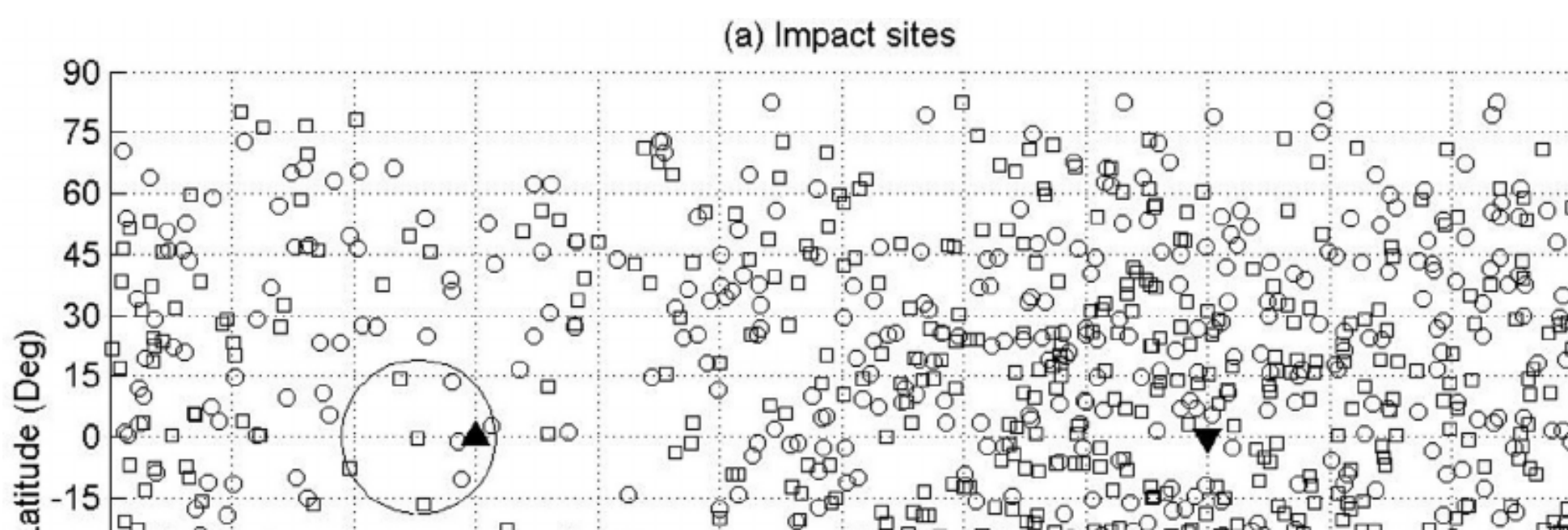
Fig. 9. (a) Simulated impact sites for the Mimas ejecta which came back after spending time orbiting Saturn. Format similar to Fig. 2. Note this is essentially the same as Fig. 12 of AZDH, but with the longitude range −180° to 180° . The large oval centered at −104° longitude, 0.0° latitude represents the outline of crater Herschel. (b) Combined distribution (spalls and rubble; simplified system) of impact sites with longitude and (c) latitude; there is a strong preference for the antapex region in the longitudinal distribution of impact sites. The plus signs represent a random distribution of latitude.
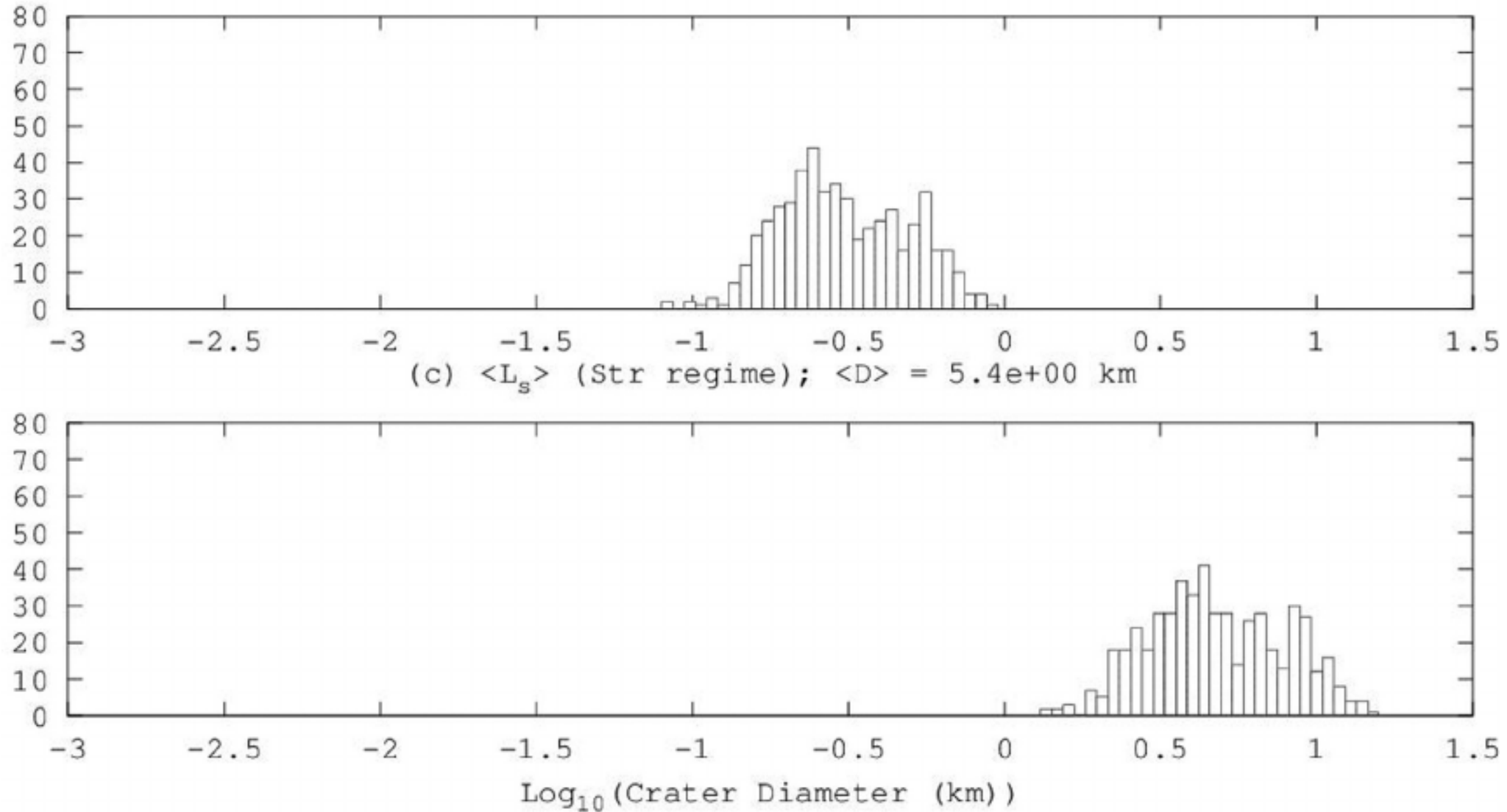
(a) L_{GK} (Str regime); $<D>$ = 4.3e-03 km

(b) Z_s (Str regime); $<D>$ = 3.4e-01 km
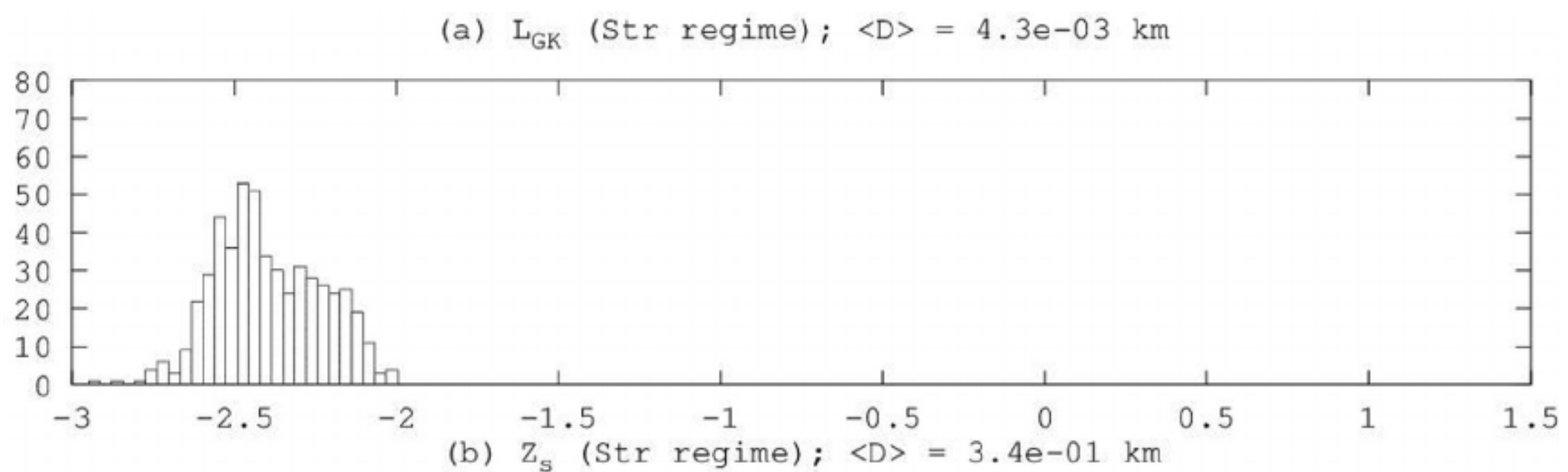
Fig. 10. SFDs of simulated sesquinary craters onto Mimas made by spall ejecta from Herschel in the strength regime (data from AZDH). Format similar to Figs. 3 and 8. Results are similar for the rubble simulation; see text for details.

from Cassini data which supersedes the Voyager coordinate system. While the 0° and 180° longitude lines are defined a priori from orbital dynamics, exact features on those points may be different and positions between them can shift. This has happened with Herschel crater, where the longitude of its center has shifted by up to 10° between the Voyager-era coordinate system and the current one.

Only public Mimas images with pixel scales better than 500 m/px that were released to PDS from the Cassini ISS instrument were used to identify craters. This allows us to cover approximately 77% of the disk and identify 10,981 impact craters. The primary gap in coverage is at the prime meridian from 20° N to the south pole. In addition, we found that the large impact crater Herschel has significantly affected the craters to within ~ 1 radius outside of its rim, and this region must be removed from any attempt to analyze the crater population longitudinally. With those caveats, we estimate that we have a complete census of craters in the regions we measured for crater diameters D > 4 km, corresponding to a minimum crater diameter of 8 pixels on the worst images used.

All craters within 135 km of 1° S −113° E (or 113° W) were removed (one crater diameter from the center of Herschel). Then, the remaining craters 4–8, 8–16, and 16–32 km were binned in 30° – wide longitude bins. If no area were removed, each bin would be equivalent to 41,316 km² (1/12 the surface area of a sphere 198.63 km in radius). However, both the area around Herschel and several areas were not included, and so the counts in each bin were normalized by the areas actually mapped.

Fig. 11 shows the results of this analysis from our database. Note that the decrease in fraction of latitude swath mapped for the −135° and −105° longitude-centered bins is due to Herschel crater. We were not comfortable attempting to reproduce the most dramatic results of LKBW, which showed a factor of 2 increase in small crater density (1.15–4.23 km) between the leading and trailing sides, with the trailing hemisphere having a larger crater density. This is because we do not think we have a complete census of craters to diameters this small that would allow such a comparison (and we might question how LKBW were able to, given the available imagery). We do show an increase in crater density between 0° and 90° E, which is the trailing portion of the near side of the satellite, by roughly 75% over the leading near side quadrant. This pattern persists through both our 4–8 and 8–16 km diameter craters, where in the latter the increase is up to 100%. This is different from what LKBW found (no significant increase nor decrease). Additionally, we found the raw crater density to be substantially higher (3x) when normalized per unit area. This further draws into question the data presented in LKBW for Mimas crater densities.

Comparing Fig. 10 with Fig. 11 suggests that few if any of the craters in the 16–32 km bin are sesquinary. However, the 8–16 and 4–8 km bins could harbor some sesquinary craters, especially the latter. Table 10 extracts the relevant statistical parameters from the

Table 10
Statistical summary for the simulated sesquinary size-frequency distributions (SFDs) in the strength regime (see Figs. 3, 8 and 10). For each source crater and scenario (leftmost column), the distribution's minimum, median, mean and maximum sesquinary crater diameters are shown, in m.

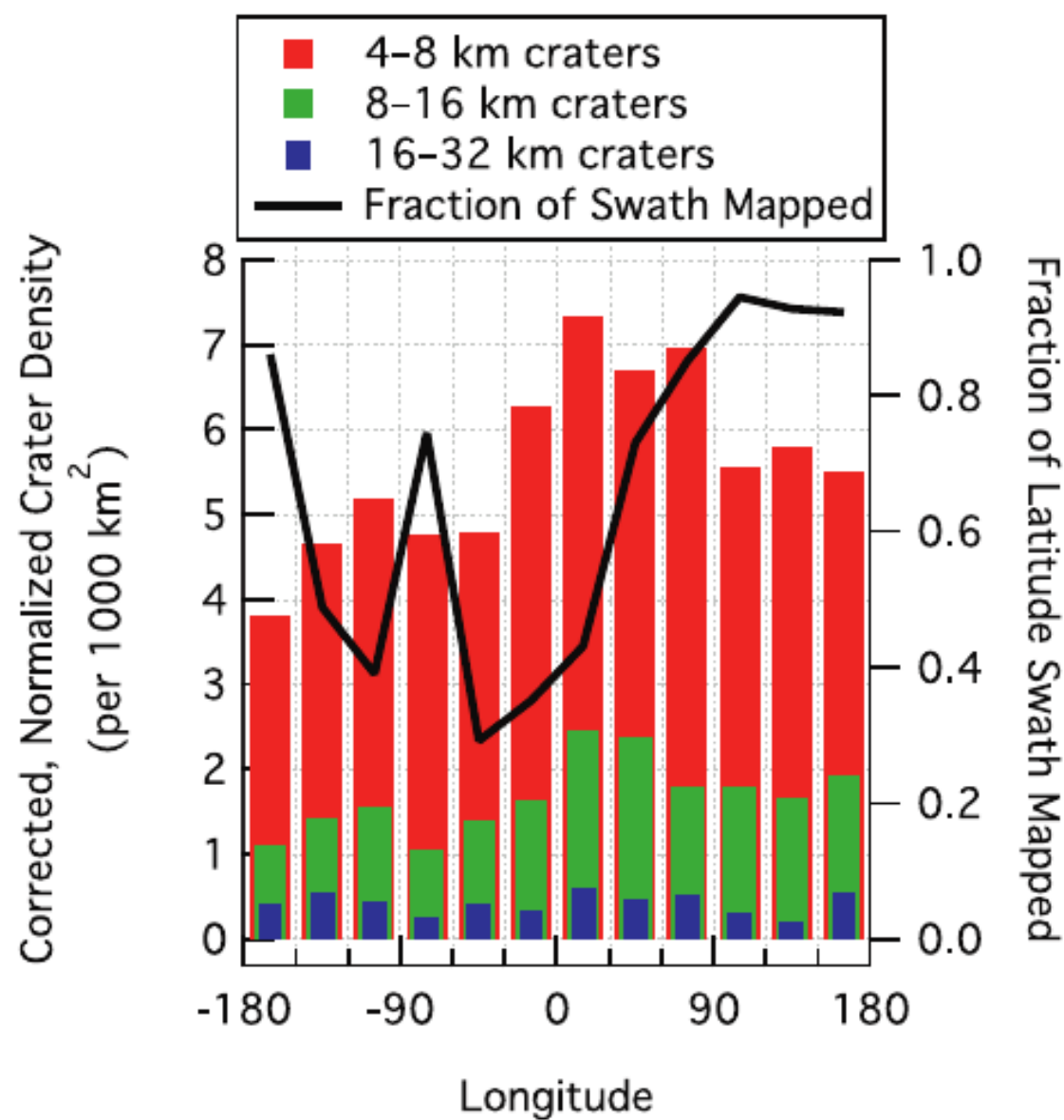| Ejecta characteristic size (m)	Herschel, Mimas	Ali Baba, Enceladus	Aeneas, Dione
Grady–Kipp	0.9,3.8,4.3,10	0.5,1.4,1.4,2.5	2.6,6.9,7.0,12
Spall thickness	80,290,340,960	22,63,65,130	81,200,210,380
Intact spalls	1300,4500,5400,16000	290,950,980,2000	1000,2800,2800,5500

Fig. 11. Density of observed craters for three size ranges on Mimas, along with completeness of coverage, as a function of longitude. Approximately 11,000 impact craters were mapped over 77% of Mimas surface. Craters within 1 crater radius of Herschel were removed (−1° latitude, 113° W longitude). Craters were separated into 4–8, 8–16, and 16–32 km diameter groups, and these were each binned in 30° – wide latitude bins. The area of these latitude bins was then calculated taking into account the actual area mapped with the Herschel impact area removed. The craters in each diameter range per each latitude bin were then scaled to yield a 'Corrected, Normalized Crater Density' per 1000 km² (left axis). The actual fraction of the entire longitude range that was mapped was also calculated and is shown by the solid black line and indicated on the right axis. This shows, for example, that only about 40% of the area between 120° and 90° W longitude was considered because of both limited image coverage and the Herschel area, while approximately 90% of the longitude swaths 90° to 180° was mapped. Note that bar graph items are superposed, not stacked.

simulated sesquinary crater size frequency distributions shown in Fig. 10; with the possible exception of the biggest sesquinary crater in the Mimas/Herschel case, all sesquinary craters are smaller than the simple-to-complex transition crater diameter (15 km). In addition, distribution parameters are also shown in Figs. 8 (Aeneas) and 3 (Ali Baba). Sesquinary craters can perhaps be distinguished by a few features such as a steep size frequency distribution, as is the case for secondary craters (e.g., McEwen and Bierhaus, 2006); the craters should be 'clean' in the sense that they would be made by the same icy material as the crust from whence they originated; the craters should be 'simple'; and finally impacts would be expected to be more oblique closer to the prime meridian, and more nearly circular near the antapex. Failure to detect a sesquinary crater signature herein would perhaps indicate that, while considerable mass is ejected into orbit about Saturn after an impact, it is mainly in the form of Grady–Kipp fragments, or even smaller particles too small to form detectable craters.

5. Discussion/Conclusions

In this paper we have analyzed the fate of escaping ejecta from craters on icy moons of Saturn: crater Ali Baba, located on Enceladus, and crater Aeneas, located on Dione. In addition we have re-examined the case of crater Herschel on Mimas (AZDH). After spending some time orbiting Saturn, most escaping ejecta come back to their source moon, thereby potentially making sesquinary craters. The impact locations of accreting ejecta are a function of the location of the source crater: in AZDH we found that most escaping ejecta originating near the apex of a synchronously rotating moon come back to near the antapex of that moon. The reverse is true for escaping ejecta originating from the antapex of a moon. However, the impact locations for ejecta originating away from these two points seems to be isotropic (see Figs. 2 and 6).

A small fraction of ejecta reaches other satellites, giving rise to the possibility of mass transfer between moons. In Alvarellos et al. (2008) we defined a 'transfer efficiency matrix' F_{jk} to express the efficiency of transferring matter from satellite j to satellite k. Given the work in AZDH and the results presented herein, we can now show an estimate for F_{jk} for the classical satellites of Saturn as (excepting Iapetus and Phoebe)

$$\begin{pmatrix} 0.97 & 0.00 & 0.00 & 0.00 & 0.00 & f_{16} & 0.00 \\ 0.02 & 0.97 & 0.03 & 0.00 & 0.00 & f_{26} & 0.00 \\ 0.00 & 0.02 & 0.89 & 0.02 & 0.00 & f_{36} & 0.00 \\ 0.00 & 0.00 & 0.07 & 0.85 & 0.03 & f_{46} & 0.00 \\ 0.00 & 0.00 & 0.00 & 0.13 & 0.93 & f_{56} & 0.01 \\ 0.00 & 0.00 & 0.00 & 0.00 & 0.03 & f_{66} & 0.78 \\ 0.00 & 0.00 & 0.00 & 0.00 & 0.00 & f_{76} & 0.05 \end{pmatrix}$$

The first column represents the fraction of *escaping* ejecta from Mimas ($k = 1$) that reach various moons. The component $F_{11} = 0.97$ represents the fraction that come back to Mimas, which is not a good scatterer of its own ejecta and is thus very efficient at cleaning up after itself. Next, $F_{21} = 0.02$ represents the fraction that reached Enceladus; etc. The next columns represent the fates of ejecta escaping Enceladus, Tethys, Dione and Rhea, respectively (data for $k = 1,3$ and 5 are from AZDH, while data for $k = 2$ and 4 are from this paper; all values are weighted averages). We have not done simulations of ejecta from Titan, so that its column remains blank above; however, Artemieva and Lunine (2005) have found that the probability of escape through Titan's thick atmosphere is rather low. The seventh column represents the fate of ejecta from Hyperion (Dobrovolskis et al., 2007; Dobrovolskis and Lissauer, 2004). At first glance it seems difficult to provide observable consequences of the matrix above, since it represents exchange of icy material between moons of very similar composition. A better, more testable prediction could come in the Jupiter system, where a big impact on Io is predicted to transport material to the surface of Europa; a thin layer of basalt on the surface of the latter would be indicative of an earlier, energetic impact on the former (Zahnle et al., 2008).

This matrix provides only a first-order approximation, since it does not take into account ejecta fates other than reaching various moons (it does not take into account the small recently discovered inner moons of Saturn, nor the integration survivors, for

instance, and with the exceptions of Enceladus and Tethys [3] it is based on single cratering events); therefore, the sum of any column components does not necessarily add up to 1.0, although in most cases it comes close to unity. Nevertheless, the matrix does contain useful information: the diagonal components are the val-

the Roche zone and hence have the potential to be tidally disrupted. The most likely eventual fate of these tidally disrupted ejecta is to hit the source moon at a later time. If the median removal time of Enceladus ejecta is 27 years, and $27/0.97 \approx 28$ years (estimated median time to be removed by Enceladus alone),

ues closest to unity, meaning that most escaping ejecta come back to the source-moon. It is interesting that both Tethys and Dione, the only two moons with coorbital companions, are more efficient scatterers than the other moons. Ejecta from Hyperion represent a break from the general trend: Hyperion is not very good at cleaning up its own debris; indeed most of it (78%) ends up in giant Titan. This is due to Titan complicating the dynamical environment of Hyperion's escaping ejecta due to the former's high mass and the 4:3 resonance between these to satellites. Perturbations due to Titan make it difficult for escaping Hyperion ejecta to return home (Farinella et al., 1990).

The removal of the population of escaping ejecta from Enceladus and Dione supports and strengthens the conclusions of Dobrovolskis et al. (2007), namely that it is best described as a stretched exponential decay, consistent with a 'spreading' process and given by Eq. (10). It is difficult to find a general trend for the time scale τ, although it roughly scales as the satellite's orbital period. As noted by Dobrovolskis et al. (2007), for Mimas, Tethys and Rhea, the parameter β seems to cluster near the value of 1/2. The examples of Enceladus and Dione also support this trend (Tables 5 and 8): averaging over these five moons the β values are 0.484 for rubble, and 0.508 for spalls. Again, note that Hyperion stands apart as in this case β is closer to 1/3 (Dobrovolskis et al., 2007), which may be due to the more complicated dynamical environment there.

Because there is uncertainty in the size scale of ejecta, we assigned sizes (given by either L_{GK}, Z_s or $\langle L_s \rangle$) to each particle. Furthermore for those that came back to their source moon, we computed not only their impact point but also their impact speed and incidence angle. Eqs. (1) and (11) give the resulting sesquinary crater diameters assuming gravity and strength regimes respectively, and from which the transition crater diameter between the two regimes can be obtained. Too anchor theoretical ejecta sizes to observations, we adopted the formalism of Singer et al. (2013), who fit power laws to observed secondary crater sizes to describe the largest possible ejecta size launched from icy satellites at any ejection velocity; for any given satellite, the largest escaping fragment will occur at $\nu_{ej} = \nu_{esc}^*$. Interestingly, the maximum ejecta size obtained thus is similar to that given by the mean spall diameter $\langle L_s \rangle$, which indicates that sesquinary craters as large as a few km in diameter, while rare, should be possible (i.e., see Figs. 3c, 8c and 10c).

For Enceladus sesquinary cratering will occur in the strength regime and will have average crater diameters between 1 and/or 65 m (depending on whether characteristic ejecta sizes given by L_{GK} or Z_s respectively), with an occasional larger sesquinary crater created by the rare large fragment of size $\langle L_s \rangle$ (average crater diameter of 980 m). In the case of larger Dione, most sesquinary craters would be created in the strength regime as well (average diameters of 7 and/or 210 m, corresponding to L_{GK} or Z_s respectively), except for the rare large sesquinary crater made by a fragment of size given by $\langle L_s \rangle$, which may occur in the gravity regime.

As proposed by BDAZ, it is also possible that the size-frequency distribution of Saturn-orbiting ejecta gets modified (i.e., the average size decreases) as a function of time due to numerous tidal encounters with moons, but mostly the source moon. We can estimate that for every ejectum that hits a satellite, about 5 more (it is an annulus, so $\approx 2.46^2 - 1^2$; Chandrasekhar, 1987) pass through

then we can estimate that once every $28/6 \approx 5$ years an ejectum from Ali Baba enters the Roche zone. Similar calculations can be performed for the other cases. Note, however, that our numerical models do not take into account tidal disruption.

Last but not least we revisit Mimas, the innermost and smallest of Saturn's classical satellites. The combination of its small size coupled with such a dominant crater as Herschel located nearly on the apex provides for an interesting scenario. Sesquinary cratering will occur unambiguously in the strength regime. If the characteristic size of the ejecta is given by L_{GK}, then sesquinary crater diameters will be about 4 m. If typical ejecta sizes are given by Z_s, the resulting average crater diameters would be about 340 m. The survey of craters on Mimas is nearly complete for diameters 4 km and larger (see caveats in Section 4.2). Therefore if ejecta fragment sizes are typically given by the Grady–Kipp scale and/or spallthickness, the resulting sesquinary crater diameters are mostly unobservable in the current Cassini data sets. The largest ejected fragment produced by the Herschel impact event would produce the largest sesquinary craters, which would average about 5.4 km, a value adjusted downward from AZDH because cratering will occur in the strength, rather than gravity, regime, while the largest possible sesquinary diameter is 16 km. Given (a) the predictions of AZDH that most escaping ejecta from Herschel that re-accrete do so near the antapex of Mimas; (b) our observational findings that indicate a greater number of small craters on the trailing side of Mimas; (c) the findings of Kirchoff and Schenk (2010) regarding the Mimas cratering record (i.e., there seem to exist two crater populations), and (d) the predictions of BDAZ (strongly supported by observations; Robbins et al., 2015) that Mimas is incapable of producing secondary craters, we propose that the most likely place to find sesquinary craters in the Saturn system (and perhaps in the whole Solar System) is near the antapex of Mimas.

Acknowledgments

References

Alvarellos, J.L., Zahnle, K.J., Dobrovolskis, A.R., Hamill, P., 2002. Orbital evolution of impact ejecta from ganymede. ICARUS 160, 108–123.

Alvarellos, J.L., Zahnle, K.J., Dobrovolskis, A.R., Hamill, P., 2005. Fates of satellite ejecta in the saturn system. ICARUS 178, 104–123.

Alvarellos, J.L., Zahnle, K.J., Dobrovolskis, A.R., Hamill, P., 2008. Transfer of mass from Io to Europa and beyond due to cometary impacts. ICARUS 194, 636–646.

Artemieva, N., Lunine, J.I., 2005. Impact cratering on titan II: global melt, escaping ejecta and aqueous alteration of surface organics. ICARUS 175, 522–533.

Batson, R.M., 1984. Voyager 1 and 2 Atlas of Six Saturnian Satellites. NASA SP-74.

Bierhaus, E.B., Dones, L., 2012. Cratering by impact ejecta, from mercury to the asteroids. In: 43rd Lunar and Planetary Science Conference. abstract 2451.

Bierhaus, E.B., Dones, L., Alvarellos, J.L., Zahnle, K.J., 2012. The role of ejecta in the small crater populations on the mid-sized saturnian satellites. ICARUS 218, 602–621.

---

3 Ejecta from craters Odysseus and Penelope; AZDH.

Buratti, B., 1999. Outer planet icy satellites. In: Weissman, P.R., McFadden, L.A., Johnson, T.V. (Eds.), Encyclopedia of the Solar System. Academic Press, San Diego,

Levison, H.F., Duncan, M.J., 1994. The long-term dynamical behavior of short period comets. ICARUS 108, 18–36.

Burns, J.A., Gladman, B.J., 1998. Dynamically depleted zones for cassini's safe passage beyond saturn's rings. Planet. Space Sci. 46, 1401–1407.

Chandrasekhar, S., 1987. Ellipsoidal Figures of Equilibrium. Dover, New York.

Chapman, C., McKinnon, W., 1986. Cratering of planetary satellites. In: Burns, J., Mathews, M.S. (Eds.), Satellites. Arizona Press, Tucson, pp. 492–580.

Dobrovolskis, A.R., Alvarellos, J.L., Lissauer, J.J., 2007. Lifetimes of small bodies in planetocentric (or heliocentric) orbits. ICARUS 188, 481–505.

Dobrovolskis, A.R., Alvarellos, J.L., Zahnle, K.J., Lissauer, J.J., 2010. Exchange of ejecta between telesto and calypso: tadpoles, horseshoes and passing orbits. ICARUS 210, 436–445.

Dobrovolskis, A.R., Burns, J.A., 1980. Life near the roche limit: behavior of ejecta from satellites close to planets. ICARUS 42, 422–441.

Dobrovolskis, A.R., Lissauer, J.J., 2004. The fate of ejecta from hyperion. ICARUS 169, 462–473.

Dones, L., Chapman, C.R., McKinnon, W.B., Melosh, H.J., Kirchoff, M.R., Neukum, G., Zahnle, K.J., 2009. Icy Satellites of Saturn: impact cratering and age determination. In: Saturn from Cassini-Huygens. Springer, pp. 613–635.

Farinella, P., Paolicchi, P., Strom, R.G., Kargel, J.S., Zappala, V., 1990. The fate of hyperion's fragments. ICARUS 83, 186–204.

Gilbert, G.K., 1893. The Moon's face: a study of the origin of its features. Bull. Phil. Soc. Washington 12, 241–292.

Hamilton, D.P., Burns, J.A., 1994. Origin of saturn's e ring: self-sustained, naturally. Science 264, 550–553.

Harper, D., Taylor, D.B., 1993. The orbits of the major satellites of saturn. Astron. Astrophys. 268, 326–349.

Horedt, G.P., Neukum, G., 1984. Cratering rate over the surface of a synchronous satellite. ICARUS 60, 710–717.

Housen, K.R., Holsapple, K.A., 2011. Ejecta from impact craters. ICARUS 211, 856–875.

Housen, K.R., Schmidt, R.M., Holsapple, K.A., 1983. Crater ejecta scaling laws: fundamental forms based on dimensional analysis. J. Geophys. Res. 88, 2485–2499.

Hsu, H.-W., Postberg, F., Sekine, Y., Shibuya, T., Kempf, S., Horányi, M., Juhász, A., Altobelli, N., Suzuki, K., Masaki, Y., Kuwatani, T., Tachibana, S. , Sirono, S.-I., Moragas-Klostermeyer, G., Srama, R., 2015. Ongoing hydrothermal activities within enceladus. Nature 519, 207–210.

Kirchoff, M.R., Schenk, P., 2010. Impact cratering records of the mid-sized, icy saturnian satellites. ICARUS 206, 485–497.

Lange, M.A., Ahrens, T.J., 1987. Impact experiments in low-temperature ice. ICARUS 69, 505–518.

Leliwa-Kopystynski, J., Banaszek, M., Wlodarczyk, I., 2011. Longitudinal asymmetry of craters' density distributions on the icy satellites. Planet. Space Sci. 60, 181–192.

McEwen, A.S., Bierhaus, E.B., 2006. The importance of secondary cratering to age constraints on planetary surfaces. Annu. Rev. Earth Planet. Sci. 34, 535–567.

Melosh, H.J., 1984. Impact ejection, spallation and the origin of meteorites. ICARUS 59, 234–260.

Melosh, H.J., 1985. Ejection of rock fragments from planetary bodies. Geology 13, 144–148.

Moore, P., Hunt, G., 1983. Atlas of the Solar System. Rand McNally and Co., London.

Morrison, D., Owen, T., Soderblom, L.A., 1986. The satellites of saturn. In: Burns, J., Mathews, M.S. (Eds.), Satellites. Arizona Press, Tucson, pp. 764–801.

Robbins, S.J., Bierhaus, E.B., Dones, L.H., 2015. Craters of the saturnian satellite system: II. Mimas and rhea. In: 46th Lunar and Planetary Science Conference. abstract 1654

Schenk, P., Hoogenboom, T., Johnson, K., 2015. Secondaries and self-secondaries on icy and small rocky bodies. Workshop on Issues in Cratering Studies and the Dating of Planetary Surfaces.

Schmidt, R.M., Housen, K.R., 1987. Some recent advances in the scaling of impact and explosive cratering. Intl. J. Impact Eng. 5, 543–560.

Shoemaker, E.M., Wolfe, R.A., 1982. Cratering timescales for the galilean satellites. In: Morrison, D. (Ed.), Satellites of Jupiter. Arizona Press, Tucson, pp. 277–339.

Sinclair, A.T., 1972. On the origin of the commensurabilities amongst the satellites of saturn. Mon. Not. R. Astron. Soc. 160, 169–187.

Singer, K., McKinnon, W.B., Nowicki, L.T., 2013. Secondary craters from large impacts on europa and ganymede: ejecta size-velocity distributions on icy worlds, and the scaling of ejecta blocks. ICARUS 226, 865–884.

Smith, B.A., et al., 1981. Encounter with saturn: voyager 1 imaging science results. Science 212, 163–191.

Smith, B.A., et al., 1982. A new look at the saturn system: the voyager 2 images. Science 215, 504–537.

Spencer, J., 2011. Watery enceladus. Phys. Today 64, 38–44.

Waite, J.H., Lewis, W.S., Magee, B.A. , Lunine, J.I., McKinnon, W.B., Glein, C.R., Mousis, O., Young, D.T., Brockwell, T., Westlake, J., Nguyen, M.J., Teolis, B.D., Niemann, H.B., McNutt Jr, R.L., Perry, M., Ip, W.H., 2009. Liquid water on enceladus from observations of ammonia and ^{40}ar in the plume. Nature 460, 487–490.

Zahnle, K., Dones, L., Levison, H.F., 1998. Cratering rates on the galilean satellites. ICARUS 136, 202–222.

Zahnle, K., Schenk, P., Levison, H., Dones, L., 2003. Cratering rates in the outer solar system. ICARUS 163, 263–269.

Zahnle, K., Schenk, P., Sobieszczyk, S., Dones, L., Levison, H.F., 2001. Differential cratering of synchronously rotating satellites by ecliptic comets. ICARUS 153, 111–129.

Zahnle, K.J., Alvarellos, J.L., Dobrovolskis, A.R., Hamill, P., 2008. Secondary and sesquinary craters on Europa. ICARUS 194, 660–674.